SOURCE LOCALIZATION OF ELECTRICAL DIPOLES IN ELECTROENCEPHALOGRAM (EEG)

by

Adil Deniz Duru

B.S. in Computer Engineering,

Istanbul University,

2000

Submitted to the Institute of Biomedical Engineering

in partial fulfillment of the requirements

for the degree of

Master of Science

in

Biomedical Engineering

Boğaziçi University

2004

ACKNOWLEDGMENTS

I am deeply grateful to my thesis supervisor Assoc.Prof. Dr. Ahmet Ademoğlu for his academic support and his friendly tolerance.

I would like to thank Prof. Dr. Tamer Demiralp from the Istanbul University Physiology Department and his neuroscience group, especially Mehmet Ergen who gave feedback while developing the Graphical User Interface.

I would like to thank Dr. Betül Baykan (Neurologist) from Istanbul University Neurology Department for her support in collecting EEG data.

I also want to thank my family for their infinite support.

ABSTRACT

SOURCE LOCALIZATION OF ELECTRICAL DIPOLES IN ELECTROENCEPHALOGRAM (EEG)

As a noninvasive neuroimaging method, the dipole source localization of brain electrical activity has a much higher temporal resolution when compared with the functional magnetic Resonance (fMRI) or Positron Emmision Tomography (PET) Imaging. It gives a direct image of the electrical events occuring in the brain. In this study, a user friendly computational system is developed for routine analysis of EEG activity, to perform electrical Dipole Source localization. The forward problem which is an essential part of source localization is solved by both the analytical and numerical methods. For the inverse problem, the Multiple Signal Classification algorithm (MUSIC) algorithm is used. The three concentric spherical shell and realistic head models which lead to analytical and numerical forward solutions, respectively are performed for different dipole parameters for evaluation and comparison. The center of gravity (COG) approximation is used for the forward solution of the Boundary Element Method. The head model is obtained by the T1 weighted average head image issued by the Montreal Neurological Institute. The graphic user interface is extremely used on epileptic data obtained from mesial temporal sclerotic patients. The results obtained are in agreement with the clinical diagnoses reached by MRI and other neurological tests.

Keywords:EEG, Dipole Source Localization, Inverse Problem, Forward problem, Boundary Element Method, MUSIC algorithm

ÖZET

Deriüstü görüntüleme metodu olarak beynin elektriksel aktivitesinin dipol kaynak yerelleştirmesi, fonksiyonel MRI ve PET ile karşılaştırıldığında zamansal çözünürlüğü daha yüksektir. Beyindeki elektriksel olayları bağıl ilişkilerle ifade etmek yerine doğrudan belirtir. Bu çalışmada, EEG de rutin analizleri, elektriksel kaynakları yerelleştirme işlemini gerçekleştiren bir arayüz geliştirildi. Kaynak yerelleştirme için gerekli olan ileri yönlü problemin çözümü analitik ve nümerik metodlar kullanılarak gerçekleştirildi. Geri yönlü problem için çoklu sinyal ayrıştırma yöntemi algoritması kullanıldı. Analitik yöntem için içiçe geçmiş üç küre, nümerik yöntem için de gerçekçi kafa modeli farklı dipol değişkenleri ile çözüldü. İleri yönlü problemde gerçekçi kafa modeli için Sınır Değer Metodunun ağırlık merkezi yaklaşımı kullanıldı. Montreal Nöroloji Enstitüsünden sağlanan T1 ağırlıklı ortalama kafa modeli, ileri model olarak kullanıldı. Grafik arayüzü MTS hastalarından elde edilen verilerle kullanıldı. Sonuçlar MRI ve diğer nörolojik testler sonucu oluşturulan tanılarla örtüşmektedir.

Anahtar Sözcükler: EEG, Dipol kaynak yerelleştirme, ileri geri yönlü problem, Sınır Değer Metodu, MUSIC Algoritması

TABLE OF CONTENTS

ACKNOWLEDGMENTS iii
ABSTRACT iv
ÖZET v
LIST OF FIGURES viii
LIST OF TABLES x
LIST OF SYMBOLS xi
LIST OF ABBREVIATIONS 1
1. INTRODUCTION 2
2. THE FORWARD PROBLEM AND ITS SOLUTION 4
2.1 The Four Concentric Spherical Shell Model 5
2.2 The Realistic Head Model 7
2.3 The Boundary Element Method 8
2.4 Discrete Approximation to Boundary Element Model 8
2.4.1 COG approximation 10
2.4.2 Calculation of the Solid Angle 11
2.4.3 Solution Of Linear Equations of BEM 12
3. INVERSE PROBLEM- Recursively Applied and Projected (RAP) MUSIC . 16
3.1 Inverse Problem 16
3.1.1 MUSIC Algorithm 20
4. IMPLEMENTATION AND RESULTS 28
4.1 Validation of Methods for the Forward Problem 28
4.2 Validation of Methods for Inverse Problem 30
4.3 Application of Simulated Data 36
4.3.1 Case:1, One Dipole 36
4.3.2 Case:2, Two Uncorrellated Dipoles 39
5. APPLICATION TO REALISTIC DATA 43
5.1 First Patient 44
5.2 Second Patient 44
5.3 Third Patient 48

6. Discussion And Conclusions 50
APPENDIX A. CODE DESCRIPTIONS 52
A.1 den1.M - Graphical User Interface 52
A.1.1 aboutApp.fig (.m) - Graphical User Interface 54
A.1.2 filterPro.fig (.m) - Graphical User Interface 54
A.1.3 useKeyBoard.fig (.m) - Graphical User Interface 55
A.1.4 mat_shell.dll - Matlab - C interface function 55
A.1.5 mat_bemforward.dll - Matlab - C interface function 55
A.1.6 mat_incogbem.dll - Matlab - C interface function 56
A.1.7 inv_main.exe - Executable code to execute calculation inversion of Solid angle matrix 57
A.1.8 mat_musicbem.dll - Matlab - C interface function 57
A.1.9 mat_musicShellW.dll - Matlab - C interface function 58
A.1.10 mat_musicShell.dll - Matlab - C interface function 58
A.1.11 mat_musicbemW.dll - Matlab - C interface function 59
A.1.12 mat_musicbemnew.dll - Matlab - C interface function 59
A.1.13 funIncRes.m -Matlab code that carries out the generation of points for the brain 60
A.1.14 mni2pixel.m -Matlab code that converts MNI coordinates to pixel coordinates 60
A.1.15 pixel2mni.m -Matlab code that converts pixel coordinates to MNI coordinates 61
A.1.16 vertplot.m -Matlab code that plots the data 61
A.1.17 xyz2pixel.m -Matlab code that converts the coordinates 62
A.1.18 mrplot.m -Matlab code plots the results of MUSIC algorithm . . 62
A.1.19 Newrapmusic.m -Matlab code that implements MUSIC algorithm 63
APPENDIX B. CD-ROM 64
REFERENCES 65

LIST OF FIGURES

Figure 2.1	Flowchart for Forward Solution	5
Figure 2.2	Concentric shells . Each shell has different conductivity values (σ_i $i = 1, 2, 3, 4$)	6
Figure 3.1	Source Localization Flowchart	17
Figure 3.2	Least Squares Method for Inverse Problem	21
Figure 3.3	Flowchart for MUSIC algorithm	25
Figure 4.1	Spherical Head Model for Analytical approach	29
Figure 4.2	Tesselated Spherical Head Model for BEM approach	29
Figure 4.3	Tessellated surface of the spherical head model with electrodes.	30
Figure 4.4	Predefined Dipole positions in the brain.	31
Figure 4.5	Mean RDM versus Eccentricity. a)Spherical Head model is tesselated with 500 triangles per surface. b)Spherical Head model is tesselated with 1000 triangles per surface. c)Spherical Head model is tesselated with 2000 triangles per surface.	31
Figure 4.6	Mean MAG versus Eccentricity. a)Spherical Head model is tesselated with 500 triangles per surface. b)Spherical Head model is tesselated with 1000 triangles per surface. c)Spherical Head model is tesselated with 2000 triangles per surface.	32
Figure 4.7	Realistic Head Model	34
Figure 4.8	Electrode Locations for the Realistic Head Model.	34
Figure 4.9	Histogram of Localization Error, dark blue bar shows Signal with no noise, light blue bar shows signal with noise (SNR=10), yellow bar shows signal with noise (SNR=6), red bar shows signal with noise (SNR=2)	35
Figure 4.10	GUI-Data Segment Selected	37
Figure 4.11	Red arrow shows the original dipole position , blue arrow shows the result of the 8 mm Voxel search.	37
Figure 4.12	Location of the source in a)Transversal, b)Saggital, c)Coronal planes and d)Moment Strength -8mm resolution	38

Figure 4.13	Location of the source in a)Transversal, b)Saggital, c)Coronal planes and d)Moment Strength -2mm resolution	39
Figure 4.14	GUI-Data Segment Selected	40
Figure 4.15	Location of the source in a)Transversal, b)Saggital, c)Coronal planes and d)Moment Strength -2mm resolution	41
Figure 4.16	Location of the source in a)Transversal, b)Saggital, c)Coronal planes and d)Moment Strength -2mm resolution	42
Figure 5.1	EEG - Filtered with bandpass filter (0-48 Hz)	44
Figure 5.2	The spike location for case 1-1. a)Transversal b)Saggital c)Coronal views d)Moment Strength	45
Figure 5.3	The spike location for case 1-2. a)Transversal b)Saggital c)Coronal views d)Moment Strength	45
Figure 5.4	EEG -Filtered with bandpass filter (0-48 Hz)	46
Figure 5.5	The spike location for case 2-1. a)Transversal b)Saggital c)Coronal views d)Moment Strength	46
Figure 5.6	The spike location for case 2-2. a)Transversal b)Saggital c)Coronal views d)Moment Strength	47
Figure 5.7	The spike location for case 2-3. a)Transversal b)Saggital c)Coronal views d)Moment Strength	47
Figure 5.8	EEG -Dipole is set to left hemisphere	48
Figure 5.9	The spike location for case 2-3. a)Transversal b)Saggital c)Coronal views d)Moment Strength	49

LIST OF TABLES

Table 4.1 Mean of Localization Error for Realistic Head model 36

LIST OF SYMBOLS

C	Deflated solid angle matrix
E	Expectation Operator
F	EEG data matrix
$H(\vec{r})$	Gain matrix for dipole located at $\vec{r}$
$H^{\dagger}$	Pseudo inverse of H
$\vec{n}$	Normal unit vector
N	Error function
N_{tr}^{l}	Number of triangles on the $l.th$ surface
$P^{\perp}$	Orthogonal complement projection matrix
r_0	Radial unit vector
R_f	Autocorrelation matrix
t_0	Tangential unit vector
P_n, P_n^1	Legendre and associated Legendre Polynomials
$\vec{r_i}$	$i.th$ Dipole location vector
$\vec{s}$	Measurement point
S_1, S_2, S_3	Surface layer of scalp, skull, brain
Δ_m^l	$m.th$ triangle of $l.th$ surface
λ_p	p.th eigenvalue
λ_{min}.	Minimum eigenvalue of the bracketed term
$\vec{\nabla}$	Gradient
ϕ_s	Eigenvectors associated with the s eigenvalues
σ_i	Conductivity of $i.th$ layer
Λ_s	Eigenvalues corresponding to signal space
$\|\|.\|\|_F$	Frobenius norm

LIST OF ABBREVIATIONS

BEM	Boundary Element Method
COG	Center of Gravity
CT	Computed Tomography
EEG	Electroencephalogram
fMRI	Functional Magnetic Resonance Imaging
LE	Localization Error
LPV	Linear Potential at Vertices
MTS	Mesial Temporal Sclerosis
MUSIC	Multiple Signal Classification
PET	Positron Emmision Tomography
RRE	Relative Residual Energy
SVD	Singular Value Decomposition

1. INTRODUCTION

The electrical potential at the surface of the scalp gives the chance to the clinicians to monitor the activity of the important cortical areas of the brain. It is extremely important for the basic and clinic neuroscience to obtain a functional picture of the 3-D brain structure in the form of a neuroimage [1]. By interpreting the EEG recordings, clinicians can make diagnosis of diseases that affect the cerebral hemispheres such as epilepsy, stroke, tumors, infection, degenerative illnesses, and delirium. It is also used to investigate brain functioning in a variety of states, such as sleep sedation/anesthesia, coma, cognition, and as a supportive evidence in the determination of death.

By assuming that the discrete EEG potentials arise from dipole sources (dipole approximation), generators of this activity can often be localized in the brain by using numerical methods. The dipole source localization process generally involves two computational tasks; i) the so called forward problem which determines the electrical/magnetic distribution of potentials on the scalp given the strenght and position of the dipole source(s), and ii) the inverse problem which estimates/updates the dipole source parameters until optimal correspondence is reached between the dipole source and the measured potential distribution on the scalp [2].

For the solution of the inverse problem, the forward problem has to be solved and the discrepancy between the computed and measured potential distribution has to be used for deciding about the way to go in the inverse direction. To solve the forward problem, one has to specify the conductivity and a geometric model for each of the anatomical structures as the brain, the skull and the scalp. Basically, there are two approaches for the forward geometry; i) the concentric homogeneous spherical shell model which involves an analytical formula for the computation of the forward problem [3] and ii) realistic head models obtained from Magnetic Resonance(MR) or Computed Tomography (CT) images and which involves a numerical computation called Boundary Element Method (BEM) [4],[5]. The reason for the choice of the spherical model

is its obvious simplicity since the potential image on the scalp due to a dipole current source located anywhere inside the brain can be computed analytically [6]. The realistic head model, on the other hand, provides a more accurate computation of the potential distribution to a given source configuration but its computational and algorithmic complexity becomes much higher because of the sophisticated techniques used in computational geometry and numerical analysis.

The goal of this thesis is to develop a user-friendly computational software system for the routine analysis of EEG activity in order to perform electrical Dipole Source Localization. For this purpose, the forward problem is solved using both the spherical shell and realistic head models [7]. The inverse problem is solved using a power spectral estimation technique called Multiple Signal Classification (MUSIC). The comparison of the analytical and realistic head models is also performed for different dipole configurations. Application to realistic data is also performed.

Outline of this thesis is as follows : In Chapter 2, the theory and the discrete solution of the forward problem are presented. Chapter 3 includes details of the dipole source localization methods and solution of Inverse problem MUSIC and Recursively Applied and Projected (RAP) MUSIC algorithms are presented. In Chapter 4, the results of simulated and real EEG data are included. In Chapter 5, the results that are obtained from the real data are presented. Finally, the discussions of the results and the conclusions obtained are given in Chapter 6.

2. THE FORWARD PROBLEM AND ITS SOLUTION

If there is a single current dipole source in the brain with strength $\mathbf{m}(\mathbf{r})$ and position $\mathbf{r}$, the potentials at P distinct electrode locations on the scalp are related to the dipole parameters by

$$\mathbf{v} = \mathbf{H}(\mathbf{r})\mathbf{m}(\mathbf{r}) \tag{2.1}$$

Here, $\mathbf{v}$ is a $P \times 1$ dimensional electrical/magnetic field vector, $\mathbf{m}(\mathbf{r})$, is the three dimensional moment vector of the dipole source at $\mathbf{r}$. $\mathbf{H}(\mathbf{r})$ is the Lead Field Matrix which is a $P \times 3$ dimensional transfer function between the dipole source paremeters and the surface measurements. $\mathbf{H}(\mathbf{r})$ is a function of geometry and the electrical/magnetic properties of the tissues as well as the dipole position and measurement site.

The forward problem has been investigated by Wilson and Bailey nearly half a century ago [8]. They derived an analytic solution relating a current dipole within a homogeneous spherical volume conductor to the electric potential at the surface of the sphere. Later, analytical solutions for the three-shell [9], and four-shell [10] spherical volume conductor were defined. The analytical formulas can be used for multi-shell spherical volume conductor models. Analytical results are obtained in these studies based on polynomial expansions and faster approximation methods are available for efficient computation of the series expansions to a sufficient accuracy [3].

In the BEM, governing differential equations are transformed into integral variables, which are applicable over the boundary surface of the region. The integrals are numerically integrated over the boundary, which is divided into boundary elements. If the boundary conditions are satisfied, a system of linear algebraic equations may be established for which a unique solution can be found.

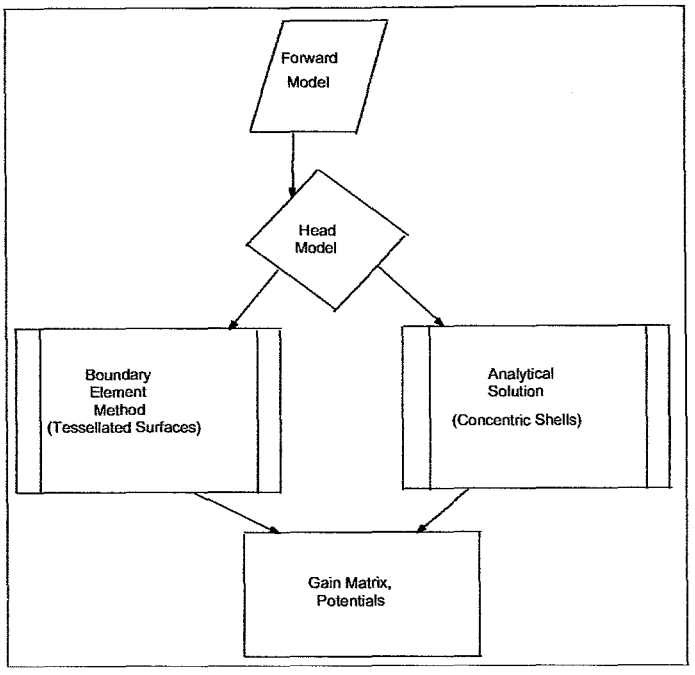

Figure 2.1 Flowchart for Forward Solution

2.1 The Four Concentric Spherical Shell Model

If the brain, cerebrospinal fluid, skull and scalp are modeled by four homogeneous concentric spherical shells with electrical conductivities σ_1, σ_2, σ_3, σ_4, respectively as shown in Figure 2.2, the electrical potential at $\mathbf{s} = [s_x s_y s_z]^T$ on the outermost shell for a dipole located ate $\mathbf{r} = [r_x r_y r_z]^T$ is

$$v(\mathbf{s}) = \frac{1}{4\pi\sigma_4 R^2} \sum_{n=1}^{\infty} c_n f^{n-1} \left[\mathbf{r}_0 P_n(\cos\theta) + \mathbf{t}_0 \frac{P_n^1(\cos\theta)}{n} \right] .\mathbf{m} \qquad (2.2)$$

Here, $\mathbf{m} = [m_x m_y m_z]^T$ is the moment of the dipole, $R = \sqrt{s_x^2 + s_y^2 + s_z^2}$, $\mathbf{r}_0 = \mathbf{r}/|\mathbf{r}|$ and $\mathbf{t}_0 = \mathbf{r} \times \mathbf{s} \times \mathbf{r}/|\mathbf{r} \times \mathbf{s} \times \mathbf{r}|$ are the radial and tangential unit vectors at $\mathbf{s}$.

$f = |\mathbf{r}|/R$ is the eccentricity of the dipole, c_n are the coefficients depending on the model geometry and conductivitites, θ is the angle between $\mathbf{r}$ and $\mathbf{s}$ and $P_n(\cos\theta)$ and $P_n^1(\cos\theta)$ are the n'th degree Legendre and associated Legendre polynomials, re-

spectively. c_n coefficients are

$$c_n = \frac{(2n+1)^4 (cd)^{2n+1}}{\Gamma} \tag{2.3}$$

$$\begin{aligned}
\Gamma \;=\; & d_{2n+1}\left[b^{2n+1}n(\frac{\sigma_1}{\sigma_2}-1)(\frac{\sigma_2}{\sigma_3}-1)(n+1)+c^{2n+1}(\frac{\sigma_1}{\sigma_2}n+n+1)(\frac{\sigma_2}{\sigma_3}n+n+1)\right]. \\
& \left[(\frac{\sigma_3}{\sigma_4}n+n+1)+(n+1)(\frac{\sigma_3}{\sigma_4}-1)d^{2n+1}\right]+ \\
& (n+1)c^{2n+1}\left[b^{2n+1}(\frac{\sigma_1}{\sigma_2}-1)(\frac{\sigma_2}{\sigma_3}n+\frac{\sigma_2}{\sigma_3}+n)+c^{2n+1}(\frac{\sigma_1}{\sigma_2}n+n+1)(\frac{\sigma_2}{\sigma_3}-1)\right]. \\
& \left[n(\frac{\sigma_3}{\sigma_4}-1)+(\frac{\sigma_3}{\sigma_4}n+\frac{\sigma_3}{\sigma_4}+n)d^{2n+1}\right]
\end{aligned} \tag{2.4}$$

Here, b, c, and d are < 1 and denote the (R) normalized radii of brain, cerebrospinal fluid and skull, respectively.

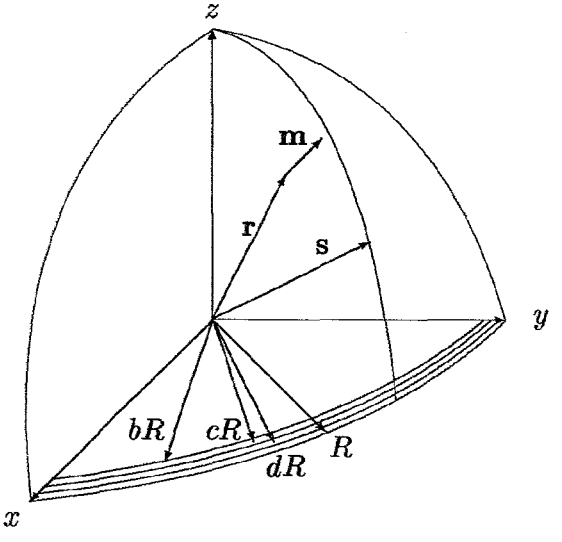

Figure 2.2 Concentric shells . Each shell has different conductivity values (σ_i $i = 1, 2, 3, 4$)

While calculating the Legendre and the associated Legendre polynomials, the

recursive formulas can be used;

$$P_{n+1}(x) = \frac{2n+1}{n+1} x P_n(x) - \frac{n}{n+1} P_{n-1}(x) \tag{2.5}$$

$$P^1_{n+1}(x) = \frac{(n+1)(P_n - xP_{n+1})}{\sqrt{1-x^2}}, for x \neq 1 \tag{2.6}$$

Initial values for Legendre Polynomials are $P_0(x) = 1$ and $P_1(x) = x$.

For the three-shell model, the algorithm can be modified by setting the radii and conductivities of the brain and the cerebrospinal fluid equal $b = c$, $\sigma_1 = \sigma_2$, respectively.

2.2 The Realistic Head Model

A realistic head model can be obtained by using medical images (CT or MR slices). To generate the realistic geometry of the brain, the skull and the scalp, the tissue boundaries are segmented on 2-D image slices either manually or by statistical means [11]. The boundaries of these segmented images are then used as contours to find a mesh of triangles covering the 3-D shell. This is called tesselation. Once the node indices and space coordinates of each triangle on every shell are determined, the realistic head model is obtained. In this study, a realistic head model is used which was previously obtained by using several segmentation and computational geometry algorithms on the T1 weighted MR images of an average human head issued by the Montreal Neurological Institute [12].

2.3 The Boundary Element Method

Once the nodal points of the tesellated surfaces are determined, a computational procedure called the Boundary Element Method is used to find the potentials on the nodes given the dipole parameters [13].

There are several approaches for the forward problem approximation. The centre of gravity of each triangle can be computed and the value of the potential at this point can be assumed to be constant over the triangle. This approximation is called the Centre of Gravity, (COG) method [4]. The potential function can be also calculated on the vertices of triangles. In this approximation, one potential value is calculated for each vertex. If the potential over a triangle is assumed to be constant and equal to the mean of the potentials at its vertices, the approximation is called as Constant Potential at Vertices, (CPV) method. On the other hand, if the potential is considered to be varying linearly over the triangle, this approximation will be called as Linear Potential at Vertices, (LPV) method [13].

The number of triangles for the head model indicates how well the true surface is approximated. The choice of method from the above models determines the number of the equations to be solved for the solution of the forward problem. For a tesselated closed surface there are about twice as many triangles as vertices. So with the same head model, there will be twice as many equations to solve if the COG approximation is used as with the CPV or LPV approximation. In this study, the COG method is adopted.

2.4 Discrete Approximation to Boundary Element Model

As the realistic head has a complex shape, a numerical method should be stated which would process the geometric data in order to solve the forward problem.

The human head can be approximated as a piecewise homogeneous conductor. For the multi layer head model, the interfaces between the regions could be denoted by S_1 , S_2 , S_3.

Based on Maxwell's equations, the relationship between sources and potential V [14] is,

$$V(\vec{s}) = V_\infty(\vec{s}) - \frac{1}{2\pi}\sum_{\ell}^{3}\frac{\sigma_\ell^- - \sigma_\ell^+}{\sigma_k^- + \sigma_k^+}\int_{S'_\ell}\vec{\nabla}'(\frac{1}{|\vec{s}-\vec{s}'|})\vec{n}(\vec{s}')dS'_\ell \tag{2.7}$$

σ_k^+, σ_k^- are the conductivity values for *kth* layer, $\vec{s}'$ is a point on the surface S_ℓ and $\vec{r}$ is a point in the volume.

σ_ℓ^- and σ_ℓ^+ are the conductivity values for the surface S_ℓ , $\vec{s}$ is a point on the S_k and $\vec{s}'$ is a point on the S_ℓ. ($\vec{\nabla}'$ means that the gradient is applied on the primed variable) $\vec{n}(\vec{s}')$ is a unit vector which is normal to the surface S_ℓ at point $\vec{s}'$ and orientation of this vector is inside to outside of S_ℓ.

$V_\infty(\vec{s})$ is the potential that is caused by a source that has a moment strength m in a conductor of infinite extend and homogeneous conductivity $(\sigma_k^- + \sigma_k^+)/2$.

$$V_\infty(\vec{s}) = \frac{1}{2\pi(\sigma_k^- + \sigma_k^+)}\int_\nu m(\vec{r}')\vec{\nabla}'(\frac{1}{|\vec{s}-\vec{r}'|})d\nu \tag{2.8}$$

In order to solve the forward problem; we should simplify the integrals of the Eq. 2.7. Calculation of surface integrals are more complex because the surfaces are irregular. Surfaces are approximated by a set of plane triangles. The surface S_ℓ can be represented by $N_{tr}^{(\ell)}$ triangles $\Delta_m^{(\ell)}$. With this surface tessellation Eq. 2.7 can be

written as

$$V(\vec{s}) = V_\infty(\vec{s}) - \frac{1}{2\pi}\sum_{\ell=1}^{3}\frac{\sigma_\ell^- - \sigma_\ell^+}{\sigma_k^- + \sigma_k^+}\sum_{m=1}^{N_{tr}^{(\ell)}}\int_{\Delta_m^{(\ell)}} V(\vec{s}')\vec{\nabla}'(\frac{1}{|\vec{s}-\vec{s}'|})\vec{n}(\vec{s}')dS' \qquad (2.9)$$

$$V_\infty(\vec{s}) = \frac{1}{2\pi(\sigma_k^- + \sigma_k^+)}\sum_{i=1}^{N_j}\frac{\vec{s}-\vec{r}_i}{|\vec{s}-\vec{r}_i|^3}m(\vec{r}_i) \qquad (2.10)$$

To calculate unknown potential function V, we must make a decision on the nodal points. We should consider that V is constant for each triangle and one value can be obtained for each triangle on its centre of gravity (COG).

2.4.1 COG approximation

As stated above in COG approximation the potential over a triangle is supposed to be constant. The nodal points are the centre of gravity of triangles. So the potential on the centre of gravity of a triangle is assumed to be same for that triangle. The integral in Eq. 2.9 can be rewritten for COG approximation.

$$\int_{\Delta_m^{(\ell)}} V(\vec{s}')\vec{\nabla}'(\frac{1}{|\vec{s}-\vec{s}'|})\vec{n}(\vec{s}')dS' = \int_{\Delta_m^{(\ell)}} V(\vec{s}')\vec{\nabla}'(\frac{1}{|\vec{s}-\vec{s}'|})\vec{n}(\vec{s}')dS' = -V(\vec{s}'_{cog})\Omega^{(l,m)}(\vec{s}) \qquad (2.11)$$

$\Omega^{l,m}(\vec{s})$ is the solid angle subtended by the triangle $\Delta_m^{(l)}$ at $\vec{s}$ and

$$\Omega^{l,m}(\vec{s}) = \int_{\Delta_m^{(\ell)}} (\frac{\vec{s}' - \vec{s}}{|\vec{s}' - \vec{s}|^3}) \vec{n}(\vec{s}') dS' \tag{2.12}$$

For COG approximation Eq. 2.9 becomes,

$$V(\vec{s}_{cog,p}) = V_\infty(\vec{s}_{cog,p}) + \frac{1}{2\pi} \sum_{\ell=1}^{3} \frac{\sigma_\ell^- - \sigma_\ell^+}{\sigma_k^- + \sigma_k^+} \sum_{m=1}^{N_{tr}^{(\ell)}} V(\vec{s}_{cog,m}) \Omega_{(\ell,m)}(\vec{s}_{cog,p}) \tag{2.13}$$

where $\vec{s}_{cog,m}$ is the centre of gravity of the m^{th} triangle $\Delta_m^{(\ell)}$ on the ℓ^{th} surface S_ℓ and p is the index for the triangle.

In the COG approximation the $\Omega_{m,m} = 0$. The rest of the solid angle subtended by the closed surface is already 2π, so there is no missing angle.

2.4.2 Calculation of the Solid Angle

One of the major steps for the solution of the BEM is the calculation of solid angles. An analytical expression of the solid angle Ω is stated by Oosterom and Strackee [15].

The solid angle subtended by a plane triangle $\Delta_m^{(\ell)}$ with the vertices $\vec{s_1}, \vec{s_2}, \vec{s_3}$ at point $\vec{s}$ can be calculated by

$$\Omega = 2 \arctan \frac{\vec{v_1}(\vec{v_2} \times \vec{v_3})}{|\vec{v_1}||\vec{v_2}||\vec{v_3}| + (\vec{v_1}\vec{v_2})|\vec{v_3}| + (\vec{v_1}\vec{v_3})|\vec{v_2}| + (\vec{v_2}\vec{v_3})|\vec{v_1}|} \tag{2.14}$$

where $\vec{v_i} = \vec{s_i} - \vec{o^*}$, for $i = 1, 2, 3$ and $\vec{o^*}$ is the origin.

The solid angle is zero when the point of view $\vec{s}$ is placed on the same plane as the triangle $\triangle_m^{(\ell)}$ exists. For the COG approximation the point of view is the centre of gravity of the triangle.

2.4.3 Solution Of Linear Equations of BEM

Eq. 2.13 can be written as,

$$v = Bv + G\bar{M} \tag{2.15}$$

$$\begin{pmatrix} v_1 \\ v_2 \\ v_3 \end{pmatrix} = \begin{pmatrix} B_{11} & B_{12} & B_{13} \\ B_{21} & B_{22} & B_{23} \\ B_{31} & B_{32} & B_{33} \end{pmatrix} \cdot \begin{pmatrix} v_1 \\ v_2 \\ v_3 \end{pmatrix} + \begin{pmatrix} G_1 \\ G_2 \\ G_3 \end{pmatrix} [\bar{M}] \tag{2.16}$$

where v_i is a vector with a length of N_{v_i} for surface S_i, it has the potential values of the nodal points. B_{ij} is a matrix with a size of $N_{v_i} \times_{v_\ell}$. It shows the influence of the potential of surface S_j on S_i. $\bar{M}$ has a size of $3N_j$. It is the moment strength matrix of sources. G_i is a matrix that has a size of $N_{v_i} \times 3N_j$. It is the free space potential matrix.

For the COG approximation the self influence matrix B is defined by

$$B_{ij}^{(p,q)} = \frac{1}{2\pi}\left(\frac{\sigma_j^- - \sigma_j^+}{\sigma_i^- + \sigma_i^+}\right)\Omega_{pq} \tag{2.17}$$

where p is the index of the nodal point on S_i , q is the index of the nodal point on surface S_j. Ω_{pq} is the solid angle at the nodal point of the p^{th} triangle of S_i subtended by the q^{th} triangle of S_j.

G is the free potential matrix can be calculated by

$$[G_{(p,x)}G_{(p,y)}G_{(p,z)}] = \frac{(\vec{s}_p - \vec{r})^t}{2\pi(\sigma_i^- + \sigma_i^+)|\vec{s}_p - \vec{r}|^3} \tag{2.18}$$

where $\vec{s}_p$ is the p^{th} nodal point on the surface S_i and $\vec{r}_q$ is the location of the q^{th} current source $\vec{j}_q$.

In Eq. 2.16, the problem is to compute the inverse of matrix $I - B$. At least one of the eigenvalues of this matrix is 0. Because matrix B has a unit eigenvalue associated with the eigenvector of [1 1 1 ... 1] with the dimension of N_{tr}. Therefore $I - B$ is rank deficient. To be able to compute the inverse of this matrix, deflation procedure was applied by Lynn and Timlake [16]. By deflation we can eliminate the null eigenvalue.

$$C^{ij} = B^{ij} - \frac{1}{N_{tr}} e_i e_j^t \tag{2.19}$$

N_{tr} is the number of triangles over all surfaces.

For a realistic head model the anatomy of brain, skull and the scalp can be considered. Conductivity values of the brain and scalp are nearly equal while the conductivity of the skull is a hundred times smaller than others. Hamalainen and Sarvas [4] noted that when the ratio of conductivity of skull to the conductivity of brain goes to zero, after deflation, the solution of Eq. 2.16 approaches to the solution of the equation for the bounded homogeneous conductor on S_3 and vanishes on the remaining surfaces. For the solution of the BEM with COG approach some extra calculations must be performed. The third equation of Eq. 2.16 is Eq. 2.20.

$$V^3 = C^{33}V^3 + G^3 + \sum_{j=1}^{2} C^{3j}V^j \tag{2.20}$$

The terms V^1 and V^2 are small according to V^3 and the accuracy of V^3 is not greatly

affected by the small value of the conductivity ratio of skull to brain. But for V^1 and V^2, we may consider V^3 as a part of the source term.

$$V^i = \sum_{j=1}^{2} C^{ij} V^j + G^i + C^{i3} V^3 i = 1, 2 \tag{2.21}$$

The source terms in Eq. 2.21 has comparatively two large parts,

$$G^i + C^{i3} V^3 \tag{2.22}$$

therefore the solution is sought in the form $V^i = W^i + W_0^i$ where $W_0^1 = W_0^2 = 0$ and W_0^3 is the potential of a homogeneous conductor bounded by S_3.

$$W^i = \sum_{j=1}^{m} C^{ij} W^j + \sigma_3^+ h^i \tag{2.23}$$

where h^i is a new source term which is defined by

$$h^1 = \frac{G^1}{\sigma_3^-} h^2 = \frac{G^2}{\sigma_3^-} h^3 = \frac{G^3}{\sigma_3^-} - \frac{2W_0^3}{\sigma_3^- + \sigma_3^+} \tag{2.24}$$

and

$$W_0^3 = \frac{\sigma_3^- + \sigma_3^+}{\sigma_3^-} G^3 + \frac{\Omega_{33}}{2\pi} W_0^3 \tag{2.25}$$

In order to solve the forward problem for realistic head model with COG approach, the first step is finding the inverse of matrix $(I - \Omega_{33})/(2\pi)$, then we can find

W_0^3 so the h^1 and h^2 and h^3 can be calculated easily. After these computations, solution of the Eq. 2.23 yields the solution of the forward problem numerically.

3. INVERSE PROBLEM- Recursively Applied and Projected (RAP) MUSIC

3.1 Inverse Problem

Infinite number of source configurations can account for the measurement of finite number of sites on the scalp [17]. Theoretically, only an infinite number of measurement sites on the surface of the brain would enable a unique determination of the locations of the responsible sources inside. To be able to find a unique solution some constraints should be set. The regions which are known that the sources do not exist can be eliminated. Therefore, the solution of the inverse problem requires the collection of sufficient information.

To localize a current dipole source by single time-slice, EEG must provide six independent views of the source at each time slice. Therefore for single time-slice localization at least six electrodes are needed. Assume that we have potential values for single time-slice denoted with $\bar{F}$, which has one column with n rows. Then the problem is to find a vector $\bar{V}$, that is generated by the predefined forward solution caused by sources whose locations are known in order to map the measured potentials. The solution for this approximation is first selecting a starting point and moving this point in the allowed locations inside the brain. So the procedure requires solving the forward problem iteratively. The aim of this algorithm is to minimize the error function.

$$J = ||\bar{F} - \bar{V}||_2 \tag{3.1}$$

Relative residual energy is defined in [18]

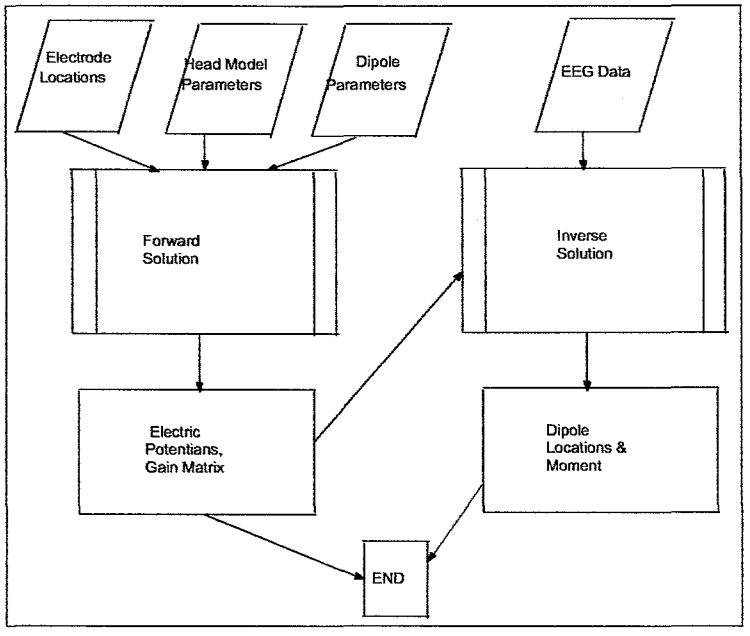

Figure 3.1 Source Localization Flowchart

$$RRE = \frac{||\bar{F} - \bar{V}||}{||\bar{V}||} \tag{3.2}$$

The solution of the inverse problem requires, moving the dipole positions iteratively. For a given dipole position r, the optimal components d in the least square sense are found from the best approximated solution of the overdetermined system of linear equations. When this function is minimized, the process of moving source stops.

$$\bar{V} = H(r).m(r) \tag{3.3}$$

Let us to call the moment $m(r)$ as M , $H(r)$ as H.

$$M = H^{\dagger}\bar{F} \tag{3.4}$$

where $H^{\dagger} = (H^t H)^{-1} H^t$ is the pseudo inverse of the lead field matrix. So relative residual energy becomes,

$$RRE = \frac{||\bar{F} - H.M||}{||\bar{F}||} = \frac{||(I - H.H^{\dagger}).\bar{F}||}{||\bar{F}||} \tag{3.5}$$

RRE depends only on the position of dipole. The solution of the dipole source localization can be found by iteratively adjusting three position parameters. For each iteration H must be computed.

Estimating the number of dipoles, their location and strength parameters using an instantaneous value of the multichannel measurement vector is known as equivalent current dipole approach. This approach requires a nonlinear optimization of $p \times 6$ number of parameters to achieve a potential distribution which fits to the measured one in the least-squares sense. Two commonly used nonlinear optimization techniques for the inverse problem are the Levenberg-Marquardt [19] and Nelder-Meade Simplex [20] algorithms. The lack of finding a unique solution following the traditional approach is partly overcome by performing nonlinear optimization using some constraints.

In multiple time-slice source localization, the sources are positioned iteratively in the head model until they account for the maximum portion of the temporal variations present in EEG. In terms of the spatiotemporal model, the EEG is described mathematically as,

$$F_i(t) = \sum_{j=1}^{p} H_{ij} m_j(t) \tag{3.6}$$

where $F_i(t)$ is the potential at electrode i at time t, m_j is the moment j and $H_{ij}(t)$ is the lead field for the j th source. p is the number of sources in the model. We can

rewrite the solution of forward problem as ;

$$\bar{V} = \bar{H}\bar{M} \tag{3.7}$$

$\bar{V}$ is the EEG data matrix with n electrodes to t time slices, $\bar{H}$ is the lead field matrix with n electrodes by p sources and $\bar{M}$ is moment matrix with p sources by t time slices.

In multiple time-slice source localization, iteration of the location parameters stops when the error function J is minimized.

$$J = ||\bar{F} - \bar{H}\bar{M}||_2 \tag{3.8}$$

The moment matrix can be written as,

$$\bar{M} = \bar{H}^{\dagger}\bar{V} \tag{3.9}$$

and by inserting Eq. 3.9 to Eq. 3.8, $\bar{M}$ can be removed from Eq. 3.8

$$J = ||(\bar{I} - \bar{H}\bar{H}^{\dagger})\bar{V}||_2 \tag{3.10}$$

To minimize Eq. 3.10, it can be seen that the pseudo inverse of H must be

calculated. To perform this computation, location of all sources should be known and the iteration for all points must be done. In this procedure mislocation of one source causes mislocation of all of them. To solve this problem a modified form of the multiple time-slice source localization method has been developed based on the multiple signal classification method called MUSIC [21],[22]. In MUSIC algorithm multiple minimum of J can be found and a new version of MUSIC which is called as recursively applied MUSIC is developed [23].

3.1.1 MUSIC Algorithm

Assume F to be the measured value from electrode sites. And $N = F - V$, where N shows the error between the measurements and calculated potentials. The measure of fit is defined as the square of the Frobenius norm

$$J_{LS} = ||F - V||_F^2 = ||F - H.M||_F^2 \tag{3.11}$$

The aim is to find the location and moment parameters that minimizes Eq. 3.11. For given location parameters and M, a solution for the matrix M that will minimize Eq. 3.11 is, $M = H^{\dagger}F$, where $H^{\dagger}$ is the pseudoinverse solution and $H^{\dagger} = V\Sigma^{+}U^{t}$, where $H = U\Sigma V^{t}$ is a singular value decomposition and Σ^{+} is the inverse of the diagonal matrix Σ. The minimization process continues for all sets of location and moment paremeters until the cost function in Eq. 3.11 minimizes.

H can be replaced by its pseudoinverse solution before solving for all parameters. The cost function in Eq. 3.11 can be defined as

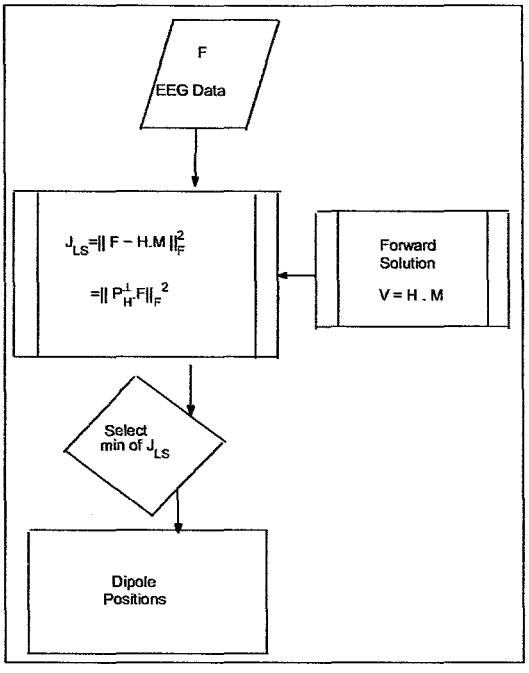

Figure 3.2 Least Squares Method for Inverse Problem

$$J_{LS} = ||F - H.M||_F^2 = ||F - H(H^{\dagger}F)||_F^2 = ||(I - P_H)F||_F^2 = ||P_H^{\perp}F||_F^2 \qquad (3.12)$$

P_H and $P_H^{\perp}$ are projection matrices. P_H projects data onto the column space of the matrix H, and $P_H^{\perp}$ is the orthogonal complement projection, that is the projection of the data onto the left null space of H. So the squared error can be computed from the projection of the data matrix F, onto the left null space.

The greatest computational complexity occurs while fitting the multiple dipole model in the iterative nonlinear minimization routine. Because of the solution of the inverse matrix problem, (solution of J_{LS}), we need to form the gain matrix H repeatedly.

If the number of time samples t, is greater than the number of sensors n, then SVD usage supplies efficiency for Eq. 3.12. So F can be written as $U\Sigma V^t$ and the cost

function in Eq. 3.12 will be $J_{LS} = ||P_H^{\perp} U\Sigma||$ because by dropping the orthogonal term V^t, result of J_{LS} does not change. While F matrix is $n \times t$, the diagonal matrix Σ should have maximum n nonzero eigenvalue thus the computation time will reduce. If rank of F is smaller than the rowsize, then savings would increase.

If SVD is used to calculate the pseudoinverse of H, then a further reduction in the number of multiplications can occur. H can be defined as $[U_a U_{n-a}]^t$, where H is n, then U_a contains the columns corresponding to the a nonzero singular values, and U_{n-a} contains the columns corresponding to the $n-a$ zero singular values where a is the rank of H. Then $P_H^{\perp} = U_{n-a} U_{n-a}^t$ so $J_{LS} = ||P_H^{\perp} W||_{n-a}^2 = ||U_{n-a}^t W||_F^2$

One of the problems of EEG dipole analysis is determining the number of dipoles. If too few are selected for any of the models, then the calculated dipoles are biased by the missing dipoles; if too many dipoles are specified, then spurious dipoles are introduced, which may be indiscernible from the true dipoles. Number of dipoles is determined by the rank of the data matrix F.

The first step is to find the gain matrix H, whose orthogonal subspace projector $P_H \perp$ minimizes J_{LS}.

The next step is to find the best orthogonal projector $P^{\perp}$, regardless of the gain matrix and then find the gain matrix H that best fits this projector. The first process in this step is to minimize over all possible orthogonal projectors of rank $n-a$ for which the first cost function is $J_1 = ||P^{\perp} F||$. Minimizing J_1 over all $P^{\perp}$ is equivalent to finding the best rank a projections of F. The best rank a approximation of F is formed by the first a components of the SVD. So if we decompose F as $F = U^t = [U_a U_{n-a}^t]$, then U_a contains the left singular vectors associated with the a largest singular values and U_{n-a} contains the remaining $n-a$ left singular vectors. The best rank a approximation of F is given by $F_a = (U_a U_a^t) F$. The best orthogonal projector is $P^{\perp} = U_{n-a} U_{n-a}^t$.

After calculation of $P^{\perp}$, next process is finding the matrix that is most orthogonal to the projector. Orthogonality between $P^{\perp}$ and H, requires each H_i to be

orthogonal with $P^{\perp}$. H_i is the gain matrix $n \times 3$ for a single dipole.

$$J_f(i) = \frac{||P^{\perp} H_i||_F^2}{||H_i||_F^2} = ||U_{n-a}^t \tilde{H}_i||_F^2 \tag{3.13}$$

where $\tilde{H}_i = H_i / ||H_i||_F$ is the normalized gain matrix. So this scanning method requires to search over all possible one-dipole locations and calculate minimum $J_f(i)$ at each location. The general approach is to evaluate $J_f(i)$ over a fine three dimensional grid to plot its inverse, and look for p sharp spikes.

For a given three-dimensional location $\vec{r}$, $H_i(\vec{L})$ is completely specified, so we seek to minimize the cost function $J_f(i)$.

$$J_f(i) = \frac{||U_{n-a}^t H_i||_2^2}{||H_i||_2^2} = \frac{||U_{n-a}^t H_i||_2^2}{||H_i||_2^2} \tag{3.14}$$

Eq. 3.14 can be called as spectral norm and can be written as,

$$J_f = \frac{H_i^t U_{n-a}^t U_{n-a} H_i}{H_i^t H_i} = \frac{H_i^t P^{\perp} H_i}{H_i^t H_i} \tag{3.15}$$

If we replace H_i with its singular value decomposition, Eq. 3.16 will equal to Eq. 3.16.

$$J_f = \frac{V_{II_i} \Sigma_{II_i} U_{II_i}^t U_{n-a}^t U_{n-a} U_{II_i} \Sigma_{II_i} V_{II_i}^t}{V_{II_i} \Sigma_{II_i} \Sigma_{II_i} V_{II_i}^t} \tag{3.16}$$

In order to find the minimum or maximum of Eq. 3.16, we should look for the minimum or maximum eigenvalue of the $[U_{G_i}^t P^{\perp} U_{G_i}]$. For the fixed p-dipole model we except to find p locations where $J_f(i) = 0$. $J_f(i)$ can be viewed as $J_f(i) = \lambda_{min}\{U_{\Pi_i}^t P^{\perp} U_{\Pi_i}\}$.

The key assumption is that spatially distinct dipoles have linearly independent time series over the measured time segment, however no constrained is imposed on whether or not the dipole moment is rotating. The model for noiseless data with n sensors and t time slices and p elemental dipole components is $V = H.M$. The additive noise is considered temporally and spatially zero-mean white noise with variance σ^2, such that the expectation of the outer product of the n noise matrix is $E\{N(i)N(i)^t\} = \sigma^2.I$, where t is the number of time slices. This requirement may be eased by prewhitening of the data, if the noise statistics are known. Under this assumption $F = HM + N$. The spatial autocorrelation of the data is then

$$R_F = E\{F(i)F(i)^t\} = E\{[H.M(i) + N(i)].[H.M(i) + N(i)]^t\} = HR_sH^t + \sigma^2.I \quad (3.17)$$

The square symmetric matrix R_F may be written in terms of its eigendecomposition as

$$R_F = \Phi\Lambda\Phi^t = [\Phi_s\Phi_n] \begin{pmatrix} \Lambda_s & \\ & \Lambda_n \end{pmatrix} [\Phi_s\Phi_n]^t \quad (3.18)$$

where we define Λ_s as the diagonal matrix containing p largest eigenvalues and Φ_s as the matrix containing the corresponding eigenvectors. From the property of the symmetric matrices all of the eigenvalues are real. It can be seen that the eigenvalue equal to the variance of the noise repeats with multiplicity $n-p$. Accordingly $\Lambda_n = \sigma^2 I$ and Φ_n is the matrix containing the corresponding $n-p$ eigenvectors associated with the repeating eigenvalues.

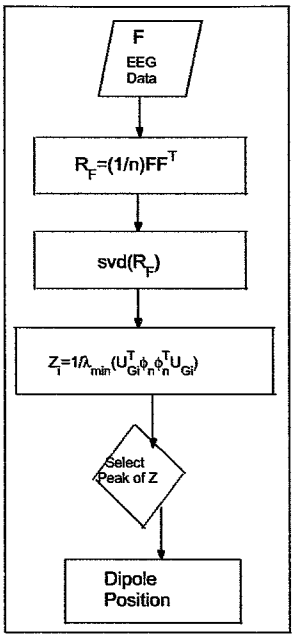

Figure 3.3 Flowchart for MUSIC algorithm

Mosher et al. [24] defined that the space spanned by Φ_s is identical to that spanned by HR_sH^t; therefore Φ_s is said to span the signal subspace. The space spanned by Φ_n is the orthogonal complement of the signal subspace and it is referred to as the noise subspace. Based on these observations $\lambda_{min}\{U_{\Pi_i}^t\Phi_n\Phi_n^tU_{\Pi_i}\}$ is zero for any matrix $H_i = U_{\Pi_i}^t\Sigma_{\Pi_i}V_{\Pi_i}^t$ corresponding to a true dipole location.

For n sensors and t time samples, F is the data matrix with the dimension of n. Then the eigendecomposition of the estimate matrix should be calculated.

$$\hat{R}_f = \frac{FF^T}{n} = \hat{\Phi}\hat{\Lambda}\hat{\Phi}^T \tag{3.19}$$

After performing SVD of F, the eigenvalues are sorted in decreasing order. $\lambda_1 \geq \lambda_2 \geq \lambda_3 \ldots \geq \lambda_m$. Signal and noise subspace of F are seperated by p. p is the number of dipoles. A distinct drop occurs between the λ_p and λ_{p+1}. Then $\hat{\Phi}_s$ and $\hat{\Phi}_n$ are defined from the corresponding signal and noise eigenvectors.

For each location on a three dimensional grid, $(x, y, z)_i$ the gain matrix H_i should

be calculated and SVD is performed on each H_i to obtain U, Σ and V. The minimum eigenvalue of the bracketed expression is found to evaluate $J_f(i)$.

$$J_f(i) = \lambda_{min}\{U_{II_i}^t \Phi_n \Phi_n^t U_{II_i}\} \tag{3.20}$$

and

$$Z(x, y, z)_i = \frac{1}{J_f(i)} \tag{3.21}$$

The maximum value of Z shows the index of the fixed dipole.

After finding the dipoles location parameters, it is easy to evaluate moment vectors from below equation.

$$F = \sum_{i=1}^{L} H(r_i, s_j) m(r_i) \tag{3.22}$$

where H is the transfer function that is generated from 3-D location vectors of i^{th} dipole and j^{th} measurement location. F is the measured data matrix and m is the strength vector.

RAP-MUSIC algorithm removes from the signal subspace the subspace associated with each source once it is found.

Finally we can summarize RAP MUSIC algorithm as,

1. Apply singular value decomposition to the $\mathbf{R_v} = (1/n)\mathbf{v}\mathbf{v}^T = \mathbf{\Phi}\mathbf{\Lambda}\mathbf{\Phi}^T$ which is generated by EEG data matrix with the dimension n and sort the eigenvalues as $\lambda_1 \geq \lambda_2 \geq \ldots \geq \lambda_n$.
2. Find a distinct drop between λ_p and λ_{p+1}, where p determines the number of dipoles.
3. For each eigenvalue (λ_1 , λ_2 , ... ,λ_p), compute data matrix by multiplying the

left and right eigenvectors with the associated eigenvalue and perform the fourth and fifth steps.

4. In a $3D$ structure, for all $\{(x, y, z)_i\}$ calculate the $\mathbf{H}$ with the dimension $n \times 3$, find the singular values of gain matrix to perform $\mathbf{H} = \mathbf{U_H}\mathbf{\Sigma_H}\mathbf{V_H}^T$. Then calculate the minimum eigenvalue of the bracketed term $J_f(i) = \lambda_{min}\{\mathbf{U_H}^T\mathbf{\Phi_n}\mathbf{\Phi_n}^T\mathbf{U_H}\}$. The spikes of $Z(x, y, z)_i = 1/J_f(i)$ gives us the position of dipoles.

5. After the localization process, it is easy to find the moments by performing Least Squares method to Eq. 2.1.

4. IMPLEMENTATION AND RESULTS

4.1 Validation of Methods for the Forward Problem

In order to show the validation of the BEM solution, a comparison between the real value and the approximated value can be made. The real value can be found by using the analytical approach Eq. 2.2 for spherical models.

Meijs et al. [25] defines the relative difference measure (RDM) and the magnification factor (MAG) to search the validation of the BEM solution.

$$RDM = \sqrt{\frac{\sum_{i=1}^{n}(V_{ana,i} - V_{num,i})^2}{\sum_{i=1}^{n} V_{ana,i}^2}} \tag{4.1}$$

where n is number of the electrodes. $V_{num,i}$ stands for the numerical solution of the ith electrode site and $V_{ana,i}$ is the real value obtained by the analytical approach.

RDM measures the level of error in the BEM solution compared to the exact analytical solution. RDM should be as small as possible. MAG is the factor that measures the relative power of the potential distribution on the scalp between the BEM and analytical solution. MAG should be one or it should remain constant for all the dipoles.

$$MAG = \sqrt{\frac{\sum_{i=1}^{n} V_{num,i}^2}{\sum_{i=1}^{n} V_{ana,i}^2}} \tag{4.2}$$

The exact solution of the forward problem can be simulated and implemented

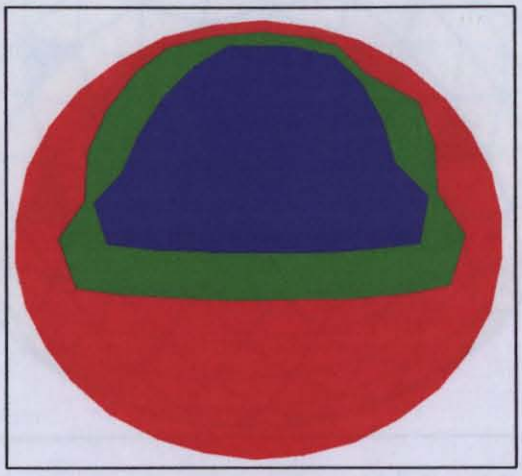

Figure 4.1 Spherical Head Model for Analytical approach

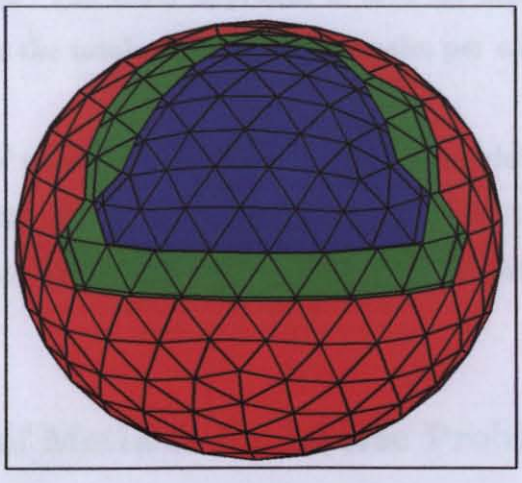

Figure 4.2 Tesselated Spherical Head Model for BEM approach

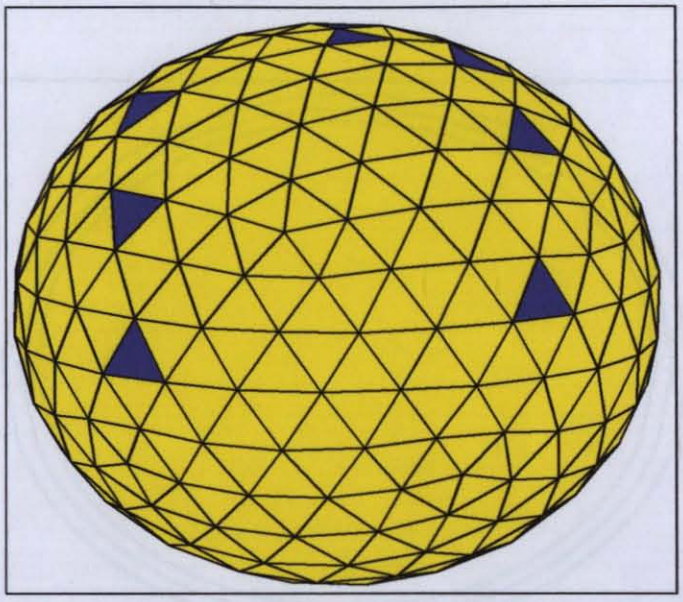

Figure 4.3 Tessellated surface of the spherical head model with electrodes.

by using Eq. 2.2. The only head model for this solution is a spherical model thus a concentric shell model with three layers is used. The head model for the BEM solution is also a three layer structure whose surfaces are tessellated where each surface has 500 triangles. Also a refined spherical head model where each of the surfaces are tesselated with 1000 triangles are used for the comparison of the number of triangles and the number of nodal points. The COG approach is used for solution so the number of nodal points is equal to the total of number of triangles per each surface.

Radius values of spherical model and tesselated model set equal for all three layers. MAG and RDM are calculated for 24312 points for the dipole locations and for 16 electrode locations the results are seen in Figure 4.5 and 4.6.

4.2 Validation of Methods for Inverse Problem

The solution of the inverse problem are tried to find by using Eq. 3.20. In order to validate this method, measured values from the electrode sites should be known. We should use sphere as a head model so that we can calculate the potentials from the

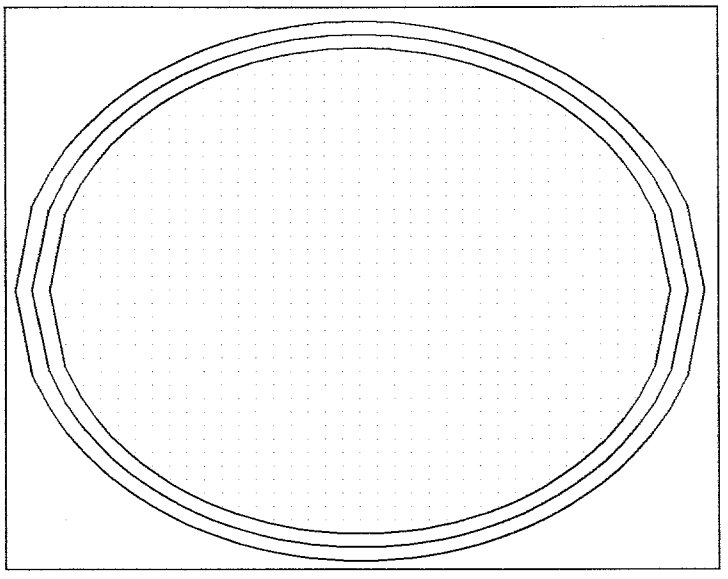

Figure 4.4 Predefined Dipole positions in the brain.

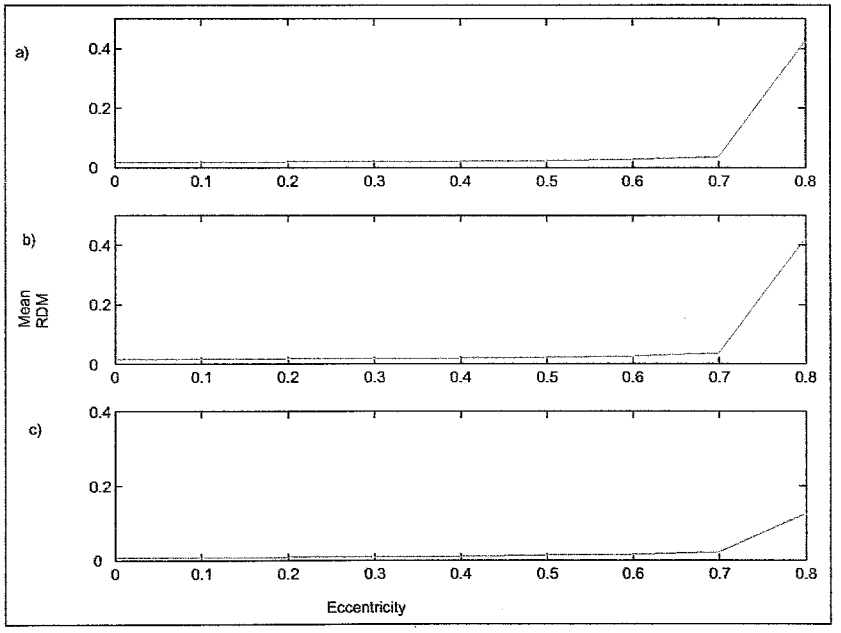

Figure 4.5 Mean RDM versus Eccentricity. a)Spherical Head model is tesselated with 500 triangles per surface. b)Spherical Head model is tesselated with 1000 triangles per surface. c)Spherical Head model is tesselated with 2000 triangles per surface.

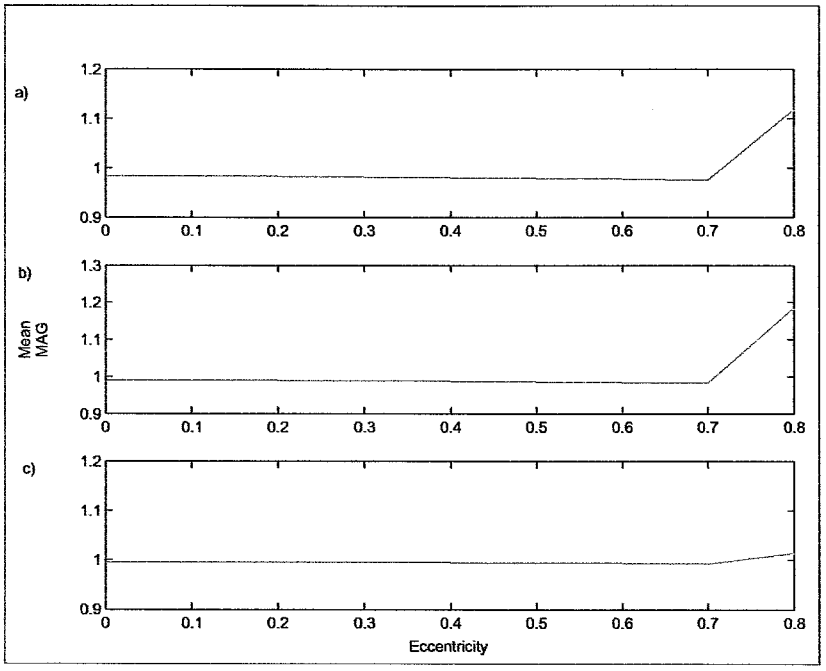

Figure 4.6 Mean MAG versus Eccentricity. a)Spherical Head model is tesselated with 500 triangles per surface. b)Spherical Head model is tesselated with 1000 triangles per surface. c)Spherical Head model is tesselated with 2000 triangles per surface.

electrode sites by using the analytical formula. From these operations simulated data is generated for each dipole position. After this process, the well known minimization procedure is applied to gather the position of the dipole. 16 electrode places are selected. 24312 locations for dipole positions are used to validate this method. To check the method which we used for inverse problem, we should look for Localization Error (LE). It is defined as,

$$LE = ||\vec{r}_f - \vec{r}_o|| \tag{4.3}$$

$\vec{r}_f$ is the result of the method and $\vec{r}_o$ is the original location. Estimation of LE is small for good accuracy. Inverse problem is solved by using above parameters.

First simulated EEG data is generated using concentric shell model for the

forward problem for each of the assumed dipole position. Then these signals are used as EEG inputs, while the forward solution that is required by the MUSIC algorithm is obtained using the concentric shell model again. At a result, there was no missing location for the predefined source positions. Mean of the localization error is zero.

At the second step, simulated EEG data is generated using BEM for the forward problem for each of the dipole locations. Then these signals are used as EEG inputs, while the forward solution that is required by the MUSIC algorithm is obtained using the BEM method again. There is no localization error in these simulations. Then EEG signal is generated by using concentric shell model and the inverse problem is solved using the BEM, again the mean of the error is zero. For the spherical model, finally EEG signal is obtained using BEM and the inverse problem is solved using the concentric shells, no localization error occured.

The forward problem is also solved for a realistic model, which was previously generated MR images of a human head issued by the Montreal Neurological Institute. Surface of the scalp is tessellated with 958 triangles, surface of the skull is tessellated with 1162 triangles and surface of the brain is tessellated with 1016 triangles. It has a total of 3136 triangles and 3037 voxels grid are selected on the brain volume for constrained localization. BEM method is used to calculate the potential over the scalp for one dipole regarding to a predefined electrode position order so a multi channel, time series are gathered for the input of the inverse problem. RAP-MUSIC algorithm is applied to this data to localize the activity. For each of the selected voxels, the forward potentials are computed and the RAP MUSIC algorithm is applied to a volume consisting of 3037 voxels with $8 \times 8 \times 8$ mm resolution. For the first case, only the input signal is used and all of the dipole positions recovered correctly by the RAP-MUSIC algorithm. The same simulation is applied by adding white gaussian noise to the simulated EEG data. Mean values of the localization error is shown in 4.1.

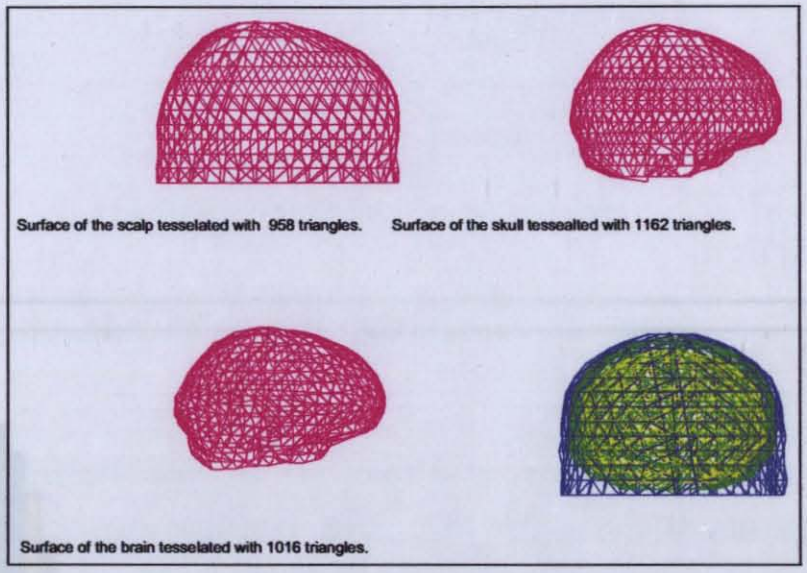

Figure 4.7 Realistic Head Model

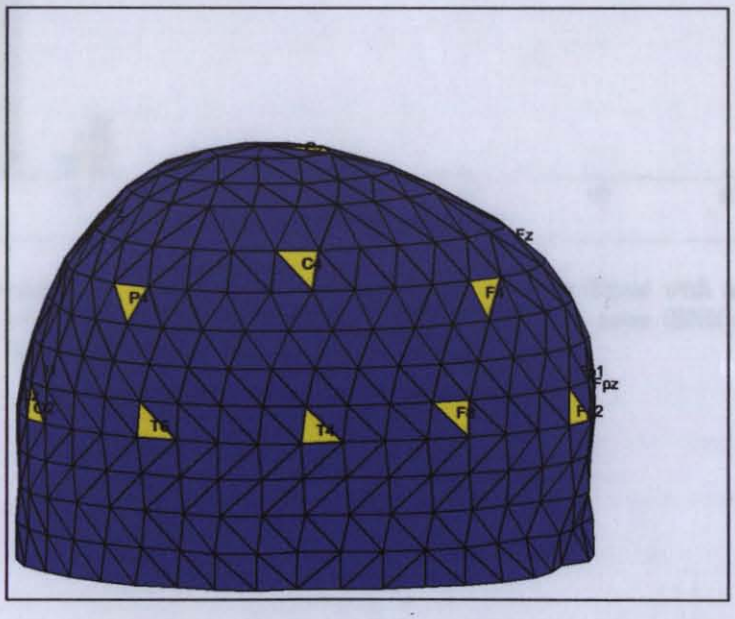

Figure 4.8 Electrode Locations for the Realistic Head Model.

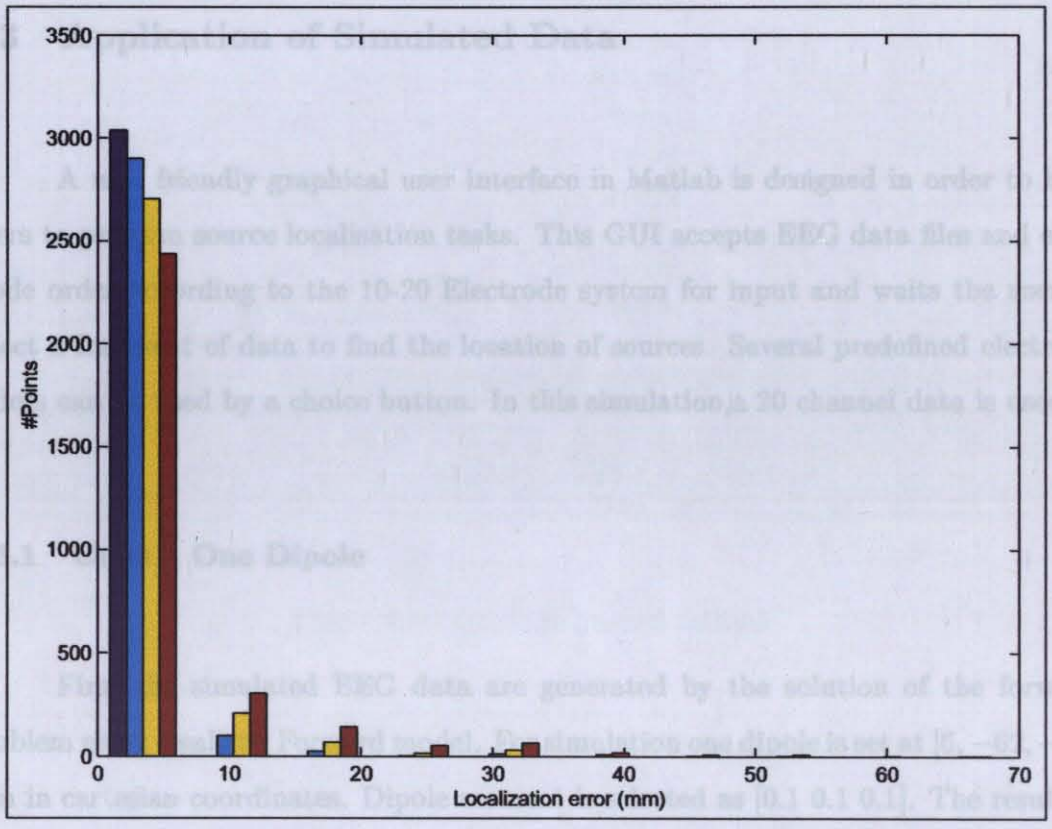

Figure 4.9 Histogram of Localization Error, dark blue bar shows Signal with no noise, light blue bar shows signal with noise (SNR=10), yellow bar shows signal with noise (SNR=6), red bar shows signal with noise (SNR=2)

Table 4.1
Mean of Localization Error for Realistic Head model

INPUT	Mean LE (mm)
BEM Signal	0
Signal+ noise ($SNR = 10$)	0.6581
Signal+ noise ($SNR = 6$)	1.775
Signal+ noise ($SNR = 2$)	3.587

4.3 Application of Simulated Data

A user friendly graphical user interface in Matlab is designed in order to help users to perform source localisation tasks. This GUI accepts EEG data files and electrode order according to the 10-20 Electrode system for input and waits the user to select a fragment of data to find the location of sources. Several predefined electrode orders can be used by a choice button. In this simulation,a 20 channel data is used.

4.3.1 Case:1, One Dipole

First the simulated EEG data are generated by the solution of the forward problem using Realistic Forward model. For simulation one dipole is set at $[6, -62, -46]$ mm in cartesian coordinates. Dipole moment is selected as [0.1 0.1 0.1]. The result of the forward solution gives us the simulated EEG data matrix.

GUI can work optionally in $8 \times 8 \times 8$ mm , or $2 \times 2 \times 2$ mm resolution. In the predefined solution set there is $8mm$ between two neighbor voxels. To increase the resolution of the solution set, after the search for the normal case, voxel found is divided into 64 new voxels with a length of $2mm$. Then localization repeated in this new gridset.

If GUI processed on $8 \times 8 \times 8$ mm resolution, the dipole would be found at $[6, -62, -48]$. MUSIC algorithm finds the nearest voxel to the dipole location.If GUI

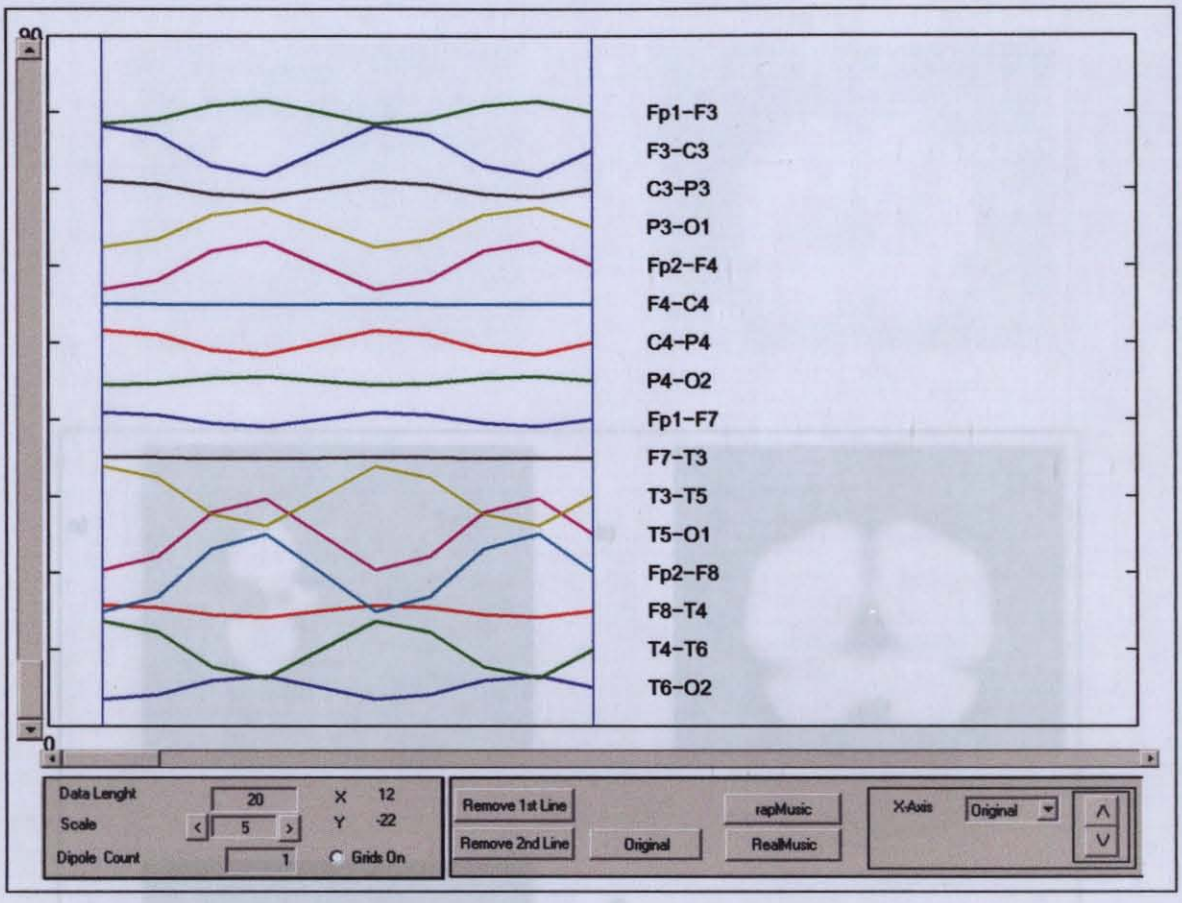

Figure 4.10 GUI-Data Segment Selected

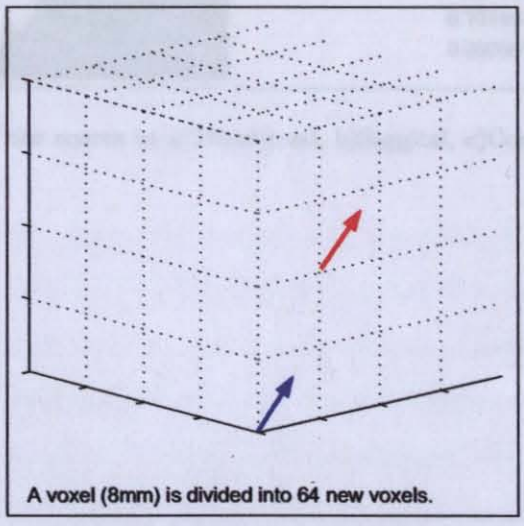

Figure 4.11 Red arrow shows the original dipole position , blue arrow shows the result of the 8 mm Voxel search.

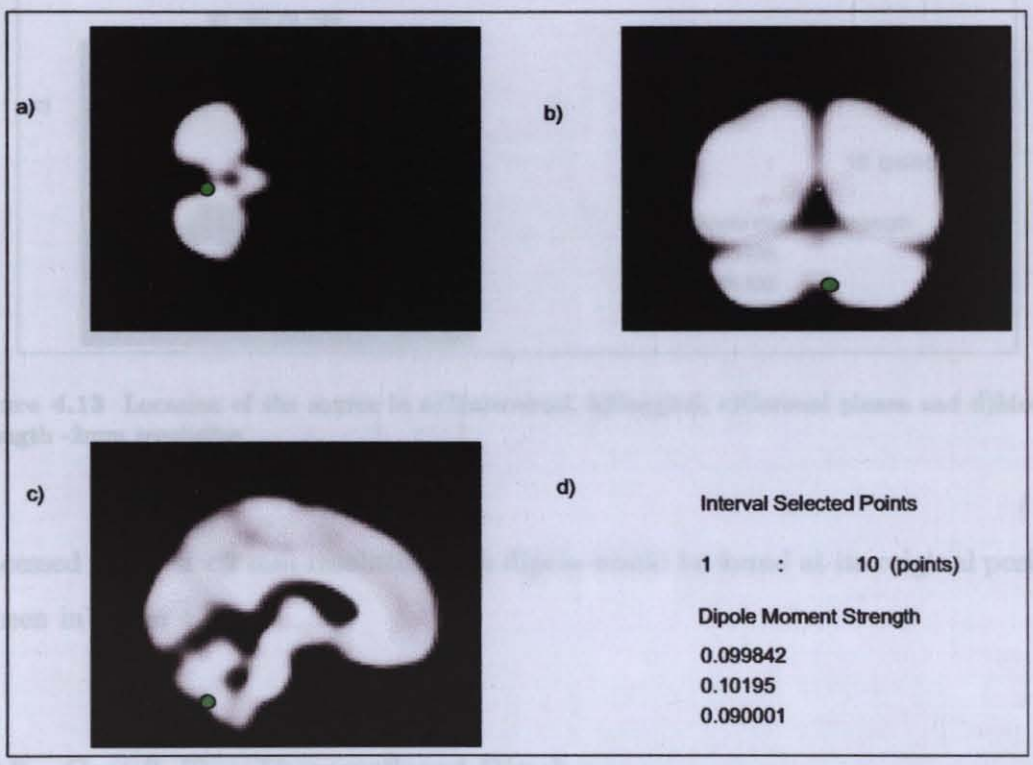

Figure 4.12 Location of the source in a)Transversal, b)Saggital, c)Coronal planes and d)Moment Strength -8mm resolution

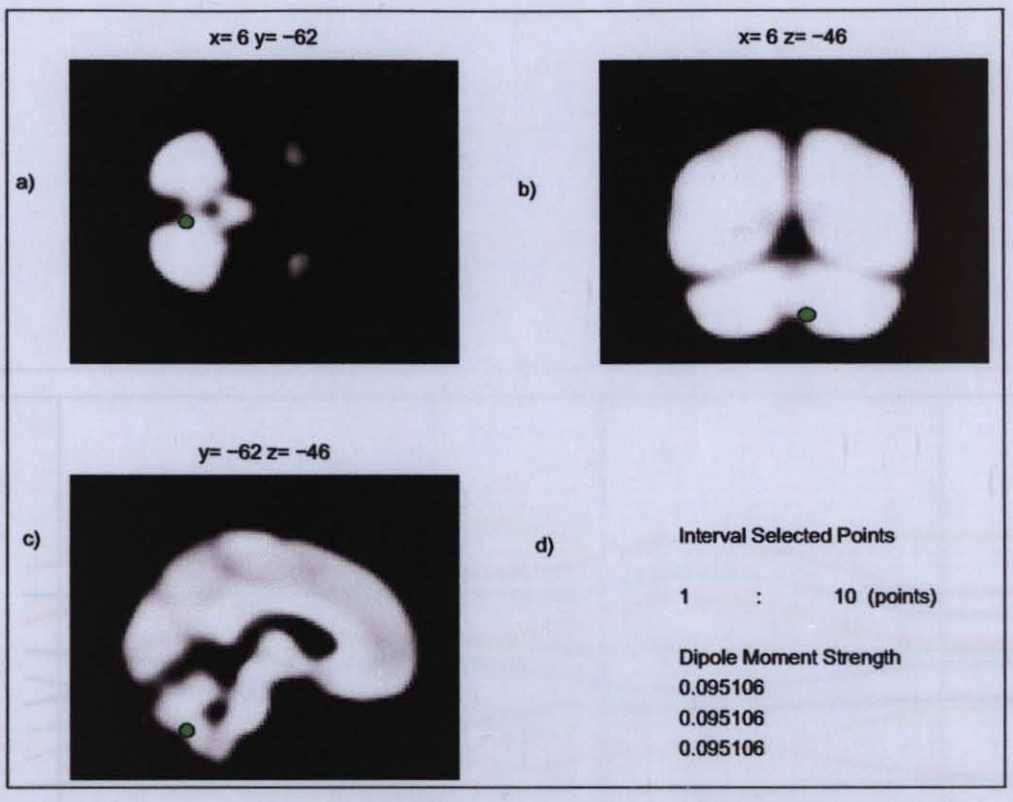

Figure 4.13 Location of the source in a)Transversal, b)Saggital, c)Coronal planes and d)Moment Strength -2mm resolution

processed on $2 \times 2 \times 2$ mm resolution, the dipole would be found at its original position as seen in figure 4.13.

4.3.2 Case:2, Two Uncorrellated Dipoles

The simulated EEG data are generated by the solution of the forward problem using Realistic Forward model. For simulation, the first dipole is set at $[-8, -44, -48]$ mm and the second dipole is set at $[22, 2, -28]$ mm in cartesian coordinates. Dipole moment is selected as [0.1 0.1 0.1]. Both of the coordinates exist in $2mm$ resolution. The result of the forward solution gives us the simulated EEG data matrix. The first part of the matrix is assigned to first dipole while the second part is for the second dipole.

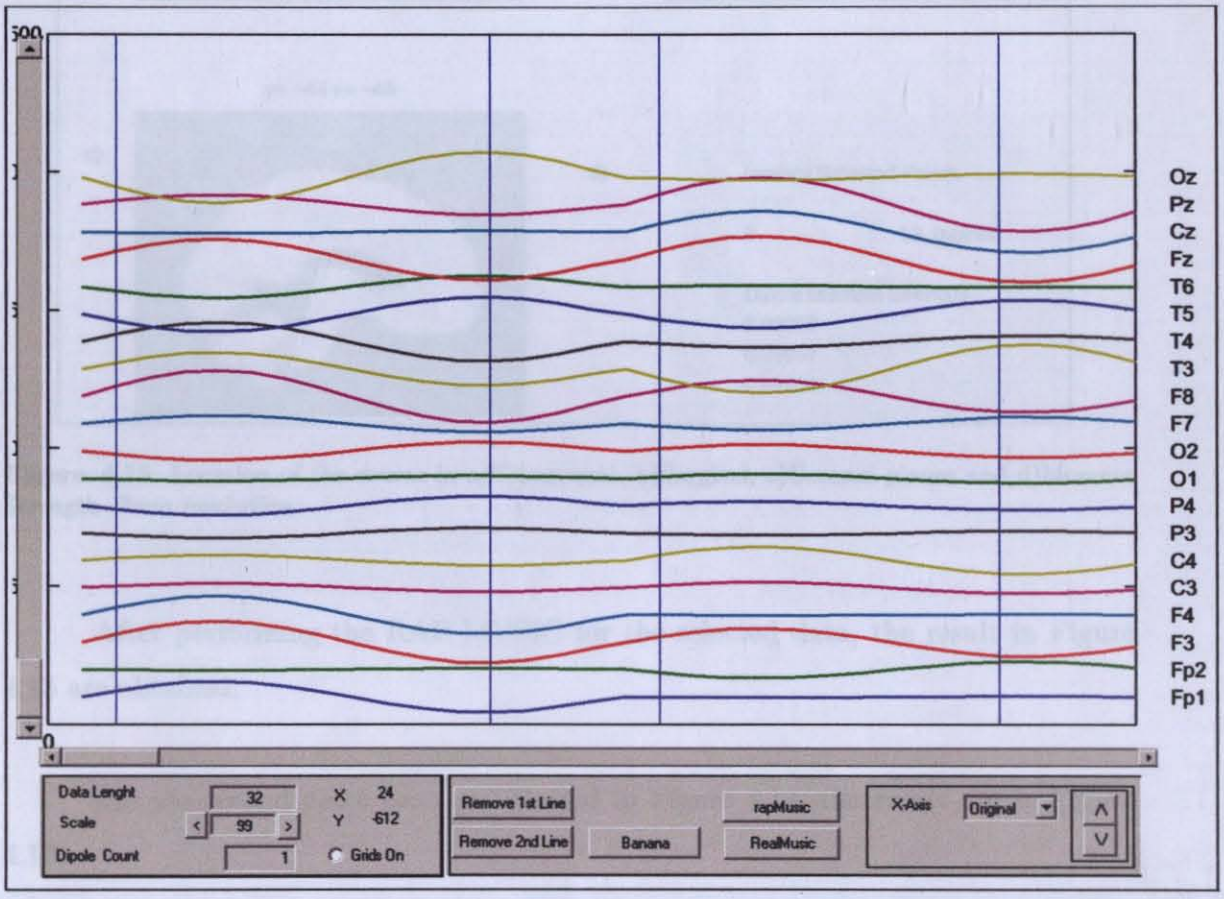

Figure 4.14 GUI-Data Segment Selected

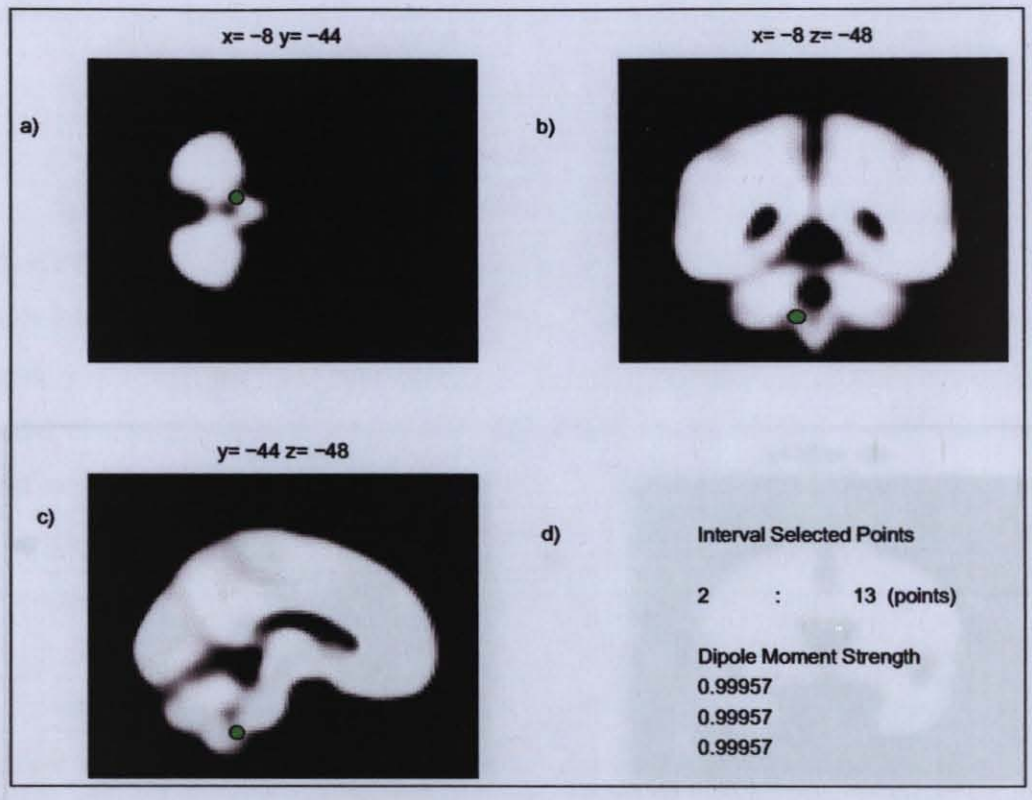

Figure 4.15 Location of the source in a)Transversal, b)Saggital, c)Coronal planes and d)Moment Strength -2mm resolution

After performing the RAP MUSIC for the selected data, the result in Figure 4.15 are obtained.

For the second spike location selected in Figure 4.14, the result are in Figure 4.16.

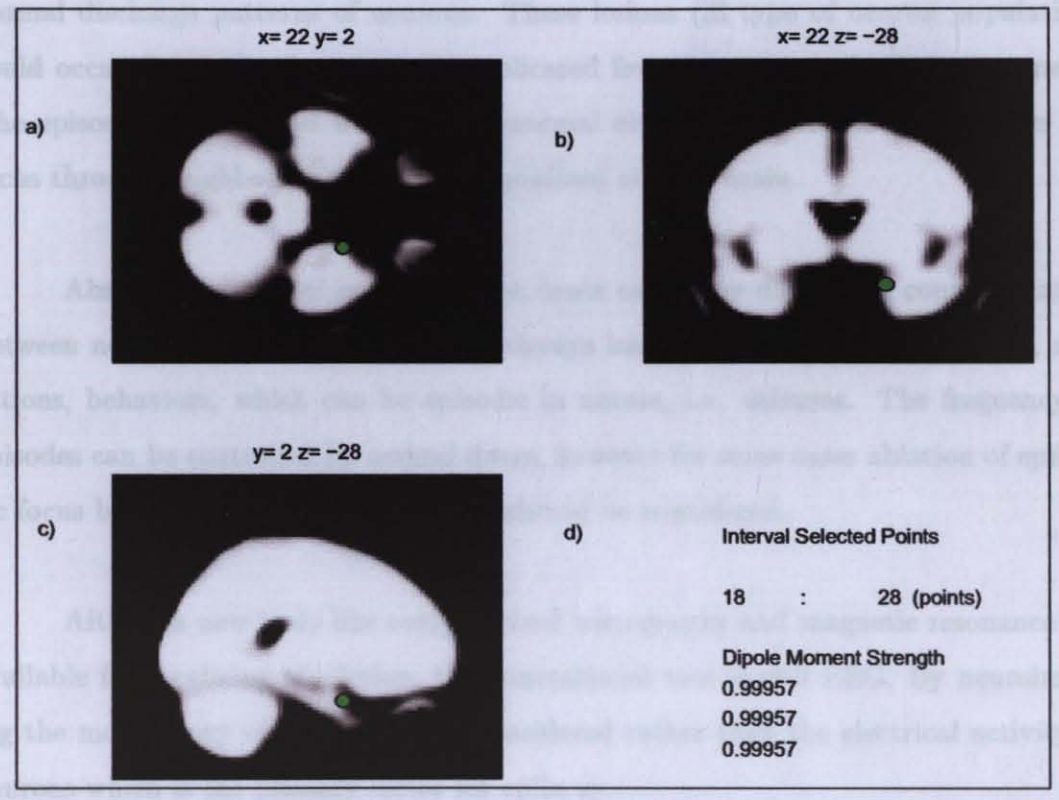

Figure 4.16 Location of the source in a)Transversal, b)Saggital, c)Coronal planes and d)Moment Strength -2mm resolution

5. APPLICATION TO REALISTIC DATA

Epilepsy is an abnormal brain activity associated with abnormal behavior, sensation, motor activity and even cognition or any combination of the above. It is commonly known as "seizure", "convulsion", "fit" or "attack". In the the cellular level, it is generally considered as abnormally facilitated excitability of neurons resulting abnormal discharge patterns of neurons. These lesions (ill type of neuron population) could occur due to head traumas, complicated fever, tumors, toxications or genetic. The episode is the period while this abnormal electrical activity is spread from the focus through neighboring tissues or generalized all over brain.

Abnormal electrical activity in the brain can cause disordered communication between neurons and along neuronal pathways leading to abnormal movements, sensations, behaviors, which can be episodic in nature, i.e. seizures. The frequency of episodes can be controlled by several drugs, however for some cases ablation of epileptic focus by neurosurgical manipulation should be considered.

Although new tools like computerized tomography and magnetic resonance are available for localizing the lesion, the conventional tool is still EEG. By neuroimaging the morphology of brain tissue is considered rather than the electrical activity of neurons which is the primary factor for epilepsy.

Temporal sclerosis or mesial temporal sclerosis (MTS) is severe loss of neurons of temporal lobe mainly over hippocampus. Typical waveform for MTS is a spike and slow wave. In this Chapter, the EEG data collected from MTS patients are analyzed by the GUI developed. The epileptic data are recorded from three different subjects from 20 electrode locations placed according to the International $10-20$ Electrode Placement System.

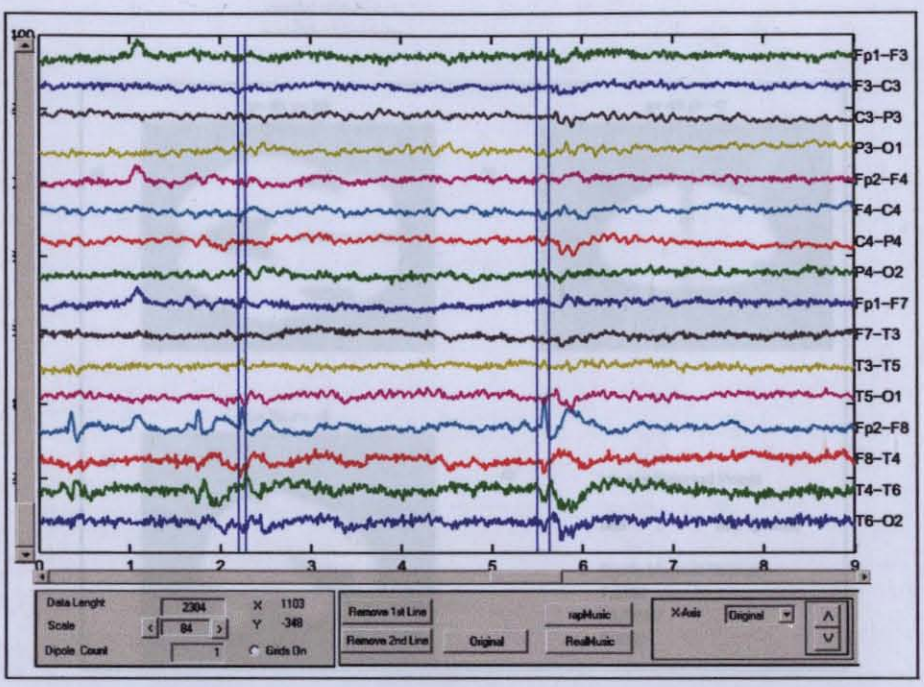

Figure 5.1 EEG - Filtered with bandpass filter (0-48 Hz)

5.1 First Patient

The first patient suffers from right MTS.

From the first data segment selected, the result of the localization algorithm is shown in Figure 5.2. For the same patient from the second data segment, the result of the localization algorithm yields the same localization.

5.2 Second Patient

The second patient suffers from the left MTS. From the first selected data segment, the result of the localization algorithm is shown in Figure 5.5. From the second data segment selected, the result of the localization algorithm is shown in Figure 5.6. From the third data segment selected, the result of the localization algorithm is shown in Figure 5.7

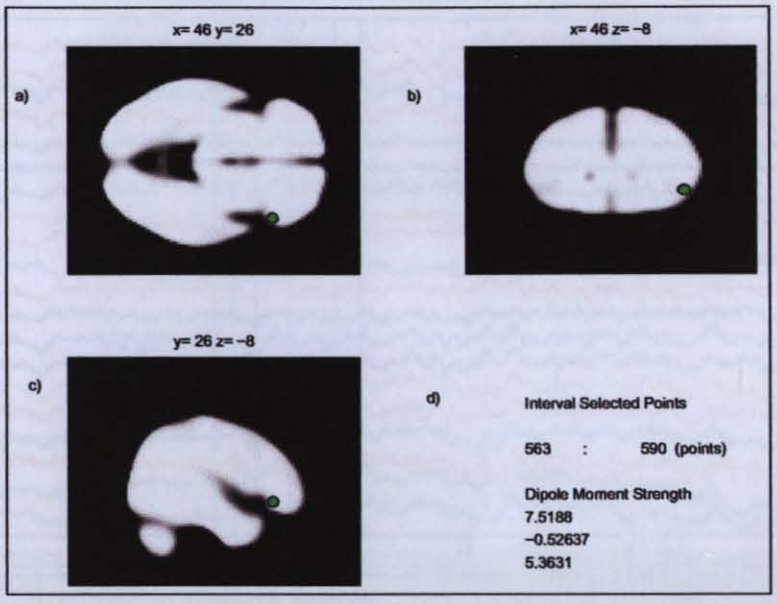

Figure 5.2 The spike location for case 1-1. a)Transversal b)Saggital c)Coronal views d)Moment Strength

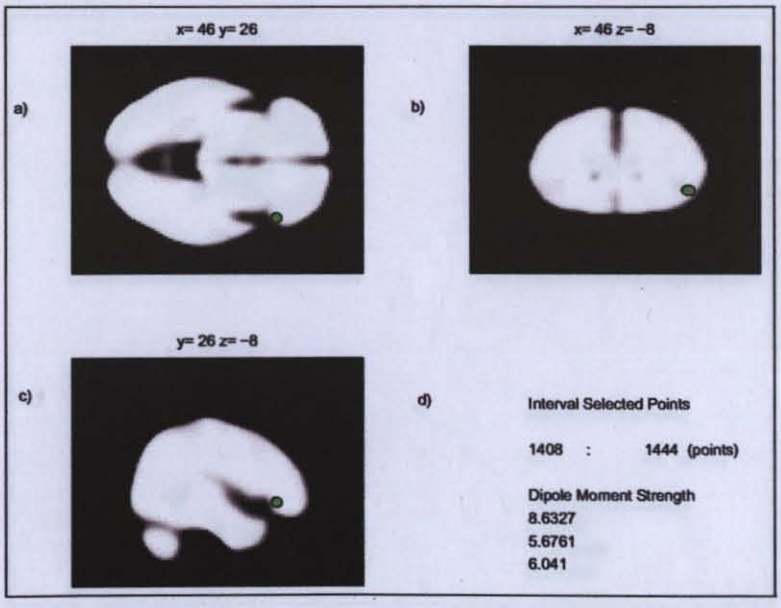

Figure 5.3 The spike location for case 1-2. a)Transversal b)Saggital c)Coronal views d)Moment Strength

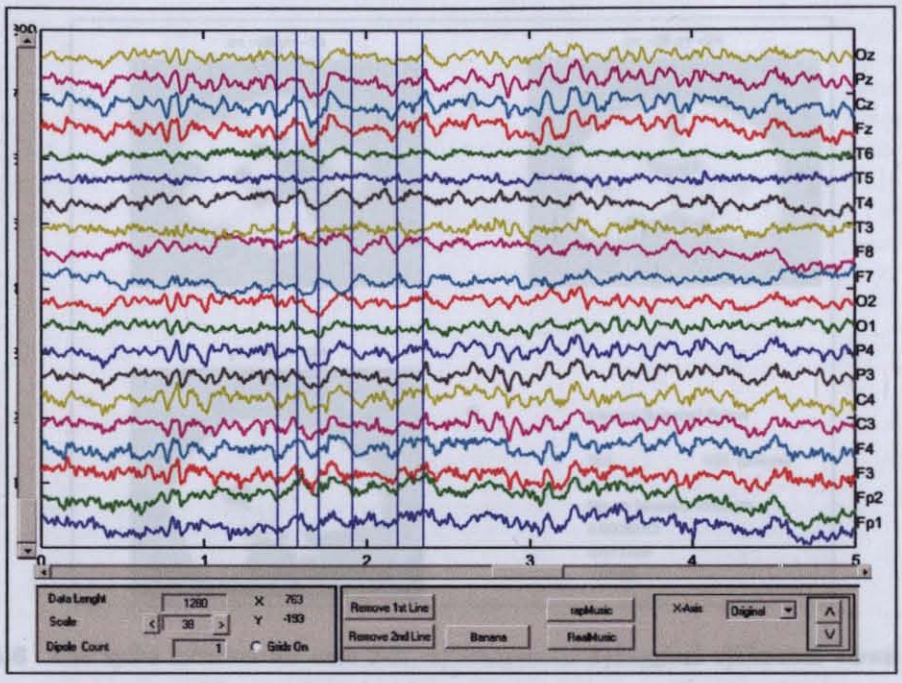

Figure 5.4 EEG -Filtered with bandpass filter (0-48 Hz)

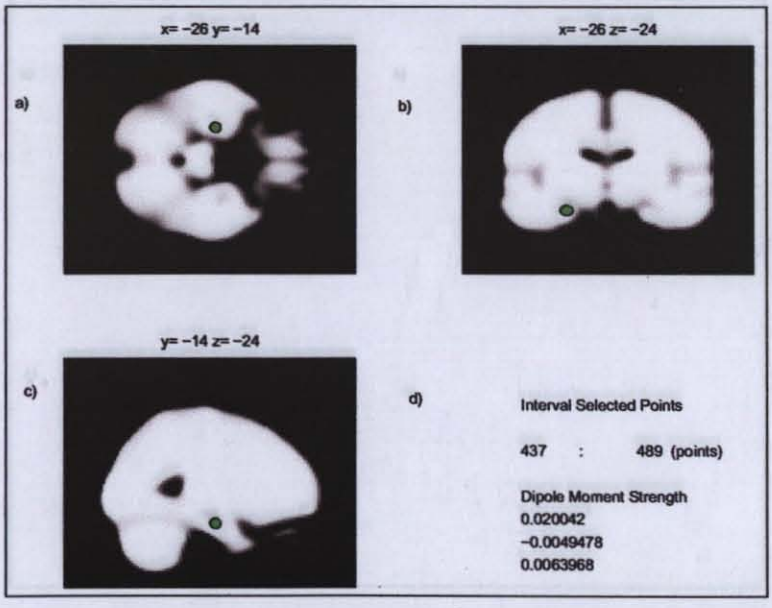

Figure 5.5 The spike location for case 2-1. a)Transversal b)Saggital c)Coronal views d)Moment Strength

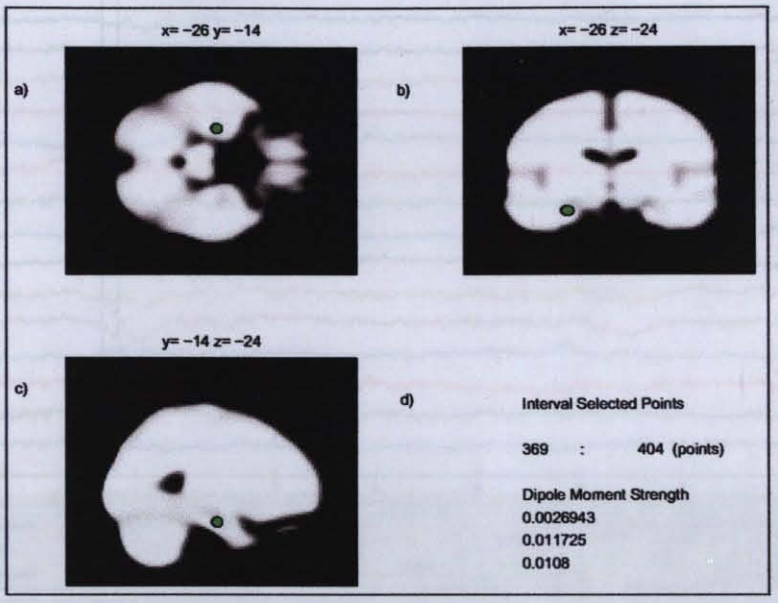

Figure 5.6 The spike location for case 2-2. a)Transversal b)Saggital c)Coronal views d)Moment Strength

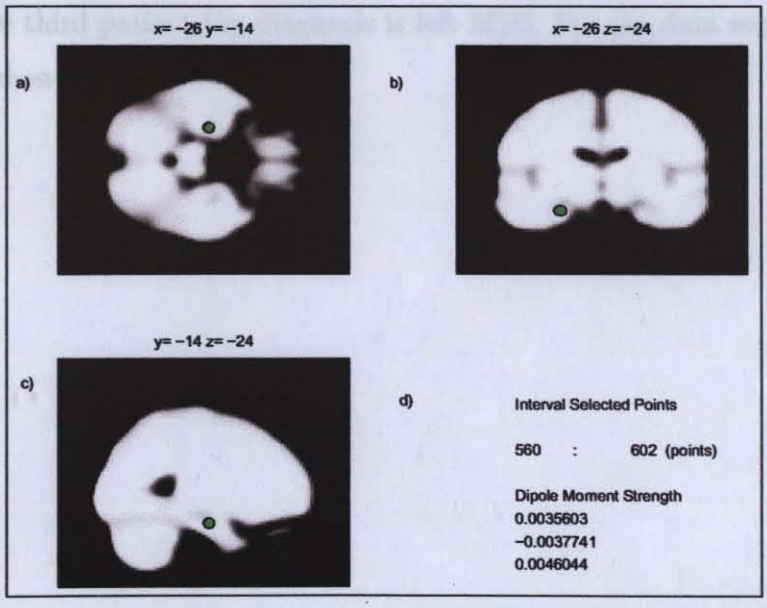

Figure 5.7 The spike location for case 2-3. a)Transversal b)Saggital c)Coronal views d)Moment Strength

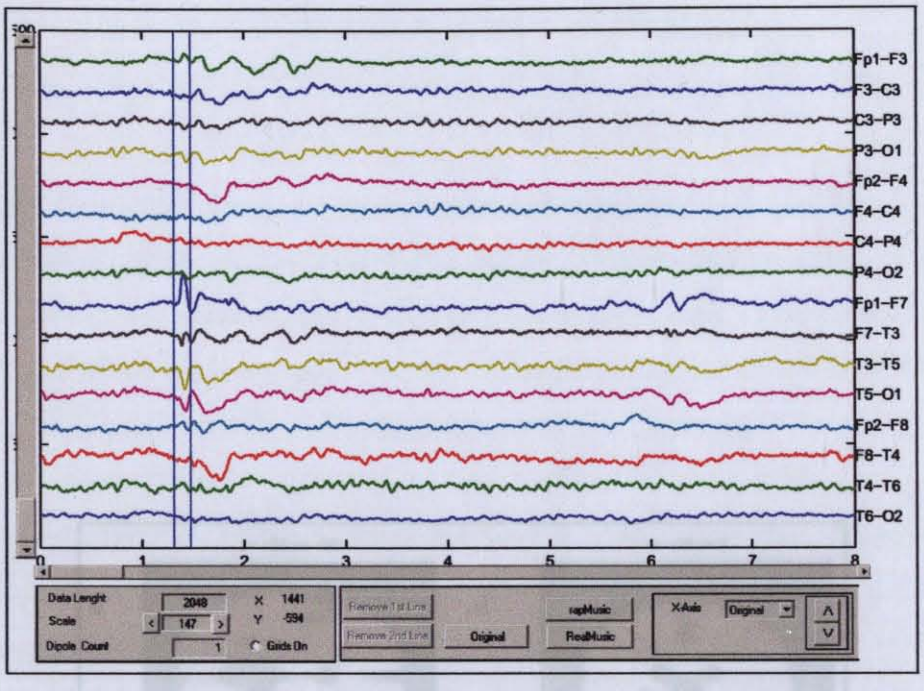

Figure 5.8 EEG -Dipole is set to left hemisphere

5.3 Third Patient

For the third patient the diagnosis is left MTS. For the data segment selected, the result is shown in Figure 5.9.

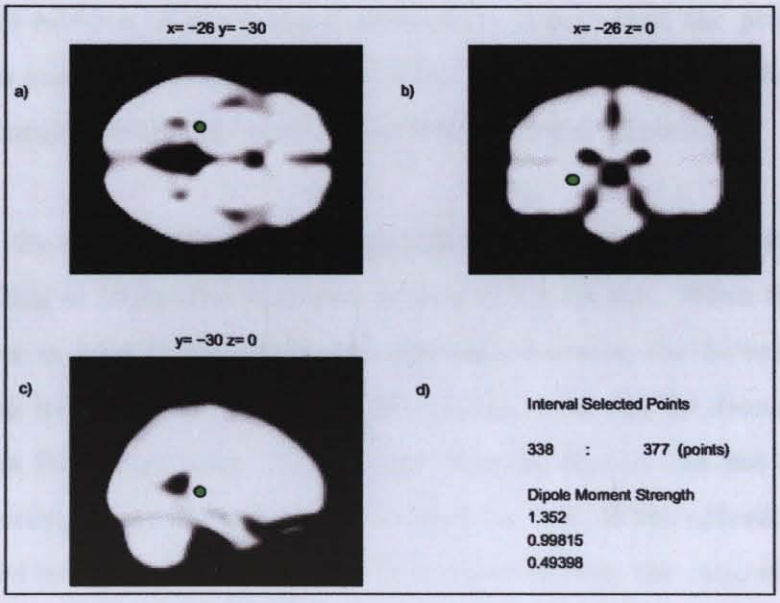

Figure 5.9 The spike location for case 2-3. a)Transversal b)Saggital c)Coronal views d)Moment Strength

6. Discussion And Conclusions

The forward problem calculation methods implemented above were applied to the spherical model shown in Figure 4.2 as well as to the realistic head model in Figure 4.7. The spherical model (concentric shells) was one of the models used since equations are available to calculate the exact values of the potentials produced by a dipole in a sphere which can be used to check the accuracy of the methods.

For the solution of the forward problem, it is seen that the properties of the selected head model plays an important role. From RDM analysis it is clear that number of triangles effects the result of the BEM forward solution.

While the eccentricity increases, the difference between the analytical approach and the solution of BEM also increases as seen in Figure 4.5. When the dipoles are located deeper or near to the origin, the difference between the forward solutions is small and can be discarded. The forward solution error can be decreased by using more triangles for the surfaces. As we know that the dipoles can not exist on CSF, meaningful eccentricity value can not be larger than 0.8. When spheres are fit to the realistic model in the least square sense, it is observed that the ratio of the radius of the brain to the radius of the scalp is 0.8. So it can be assumed that the maximum eccentricity of the dipoles has to be lower than 0.8. From Figure 4.5, there is a very small difference between the BEM and the exact solution for denser tessellated model.

It can be concluded that the use of a model with 2000 triangles per surface, will give enough accuracy for the forward problem but the increased number of triangles will bring extra computational load which may not be preferred.

The nodal points that are selected for the BEM are the COG points of the triangles. The solution for the COG approach requires the solution of the linear equations with the same size of COGs. With the same head model, if vertice based approaches

are used, the number of the equations will be half of the COG approach. However, the computation of the solid angles for the head model takes more time.

Solution of the inverse problem requires the solution of the forward problem, so the accuracy of the forward solution directly effects localization. Inverse problem can be used with both spherical and realistic forward models. The simulations showed that RAP-MUSIC algorithm is succesful while localizing the sources. When white gaussian noise is added to the original simulated EEG signal, it is seen that the mean of the localization error increases with the decreasing signal to noise ratio. By collecting sufficient information about the spatial structure, algorithm can converge faster and produce more reliable results. It is possible to increase the resolution of the solution set by splitting the voxels into desired parts. Computationally it is practical to use the $2mm$ resolution.

Further issues that can be worked on the forward problem are (i) Implementation of vertex based approach (ii) Using a higher number of triangles for the surface models.

For the inverse problem,the MUSIC and RAP-MUSIC algorithm yields satisfactory results for focal surfaces like in the case of many epileptic spikes. For the more distributed sources arising from cognitive potentials, other techniques based on Bayesian statistical inference may be used.

APPENDIX A. CODE DESCRIPTIONS

In this appendix, the names of the files found in Appendix B (CD-ROM) are outlined.

A.1 den1.M - Graphical User Interface

Source localization process is computed by this interface. This GUI accepts multi channel EEG data as a binary file, lets to select a part of it in order to perform the computations needed to localize the sources and plots them to the screen.

A binary profile file which has a '.pro' extension should be created to inform the order of the EEG channels to the gui. By this parameter flexibility of the code is increased. Several different orders can be used to compute the processes.

Data file should have the extension '.dat'. The channel dimension of the data must match the dimension of the profile file. Both profile and data file can be selected in any time after the loading of the gui by the help of menus.

Two types of the plotting exists. First one is the order that the profile file shows and second one is the Banana order which shows the potential differences between predefined electrodes. Switching between these orders can be easily made by a button.

For source localization process, a segment of the EEG data can be selected using the mouse right click command on the data. This operation should be used twice in order to generate a data block for further processing. To clear the selected block from the memory, buttons on the gui can be used. It is clear that we can not select a new data block unless we delete the old one.

Selected data points can be parameters for MUSIC algorithms using the 'Rap-Music' and the 'RealMusic' commands. Rest of the repetitive processes are computed by the below functions and procedures.

Inputs : None from command line but accepts inputs from files.

1-InitialVars.mat : Sampling rate of the EEG data, Estimated number of dipoles, Scale of the vertical axis between two adjacent channels, The length of an edge of a voxel for Localization process.

2-tdres0102.mat : Stores the name of the previously used profile file.

3-tdres0101.mat : Stores the name of the previously used data file.

4-tdresf01.mat : The name pointer of the data file which contains the singular value decomposition of the calculated gain matrices according to the profile order and the geometry values of the forward problem.

5-OrgOrderVar.mat : Contains the original order of the electrodes.

6-mus_bemNew_parameters : Contains parameters for the solution of the forward problem (BEM-COG), and the parameters that are needed for inverse problem.

Outputs :Position of the dipoles and associated moments.

Calls : aboutApp.m, useKeyBoard.m, filterPro.m, newrapmusic.m, realmusic.m, vertplot.m

Called by :None

A.1.1 aboutApp.fig (.m) - Graphical User Interface

Contains information about the current process. Shows EEG sampling rate, estimated dipole count, scale of the vertical axes, edge length of a voxel and compares the selected profile with the original electrode order. It also lets to change sampling rate, estimated dipole count, scale value and the voxel size for further processing.

Inputs : InitialVars.mat

Outputs:None

Calls : None

Called by : den1.m

A.1.2 filterPro.fig (.m) - Graphical User Interface

Sends the input parameters to the bp1.m code so that the data can be filtered according to defined characteristics.

Inputs : Filter type and properties

Output : Filtered data

Calls :bp1.m, filt.m

Called by : den1.m

A.1.3 useKeyBoard.fig (.m) - Graphical User Interface

Gets the time indexes of the data and sends the generated data segment to the MUSIC algorithm.

Inputs : Time indexes of data

Output :Dipole positions

Calls :realmusic.m

Called by :den1.m

A.1.4 mat_shell.dll - Matlab - C interface function

Implement the analytical solution for the forward problem over a sphere.

Inputs : r, double matrix $(P \times 3)$ for the position coordinates of q dipoles (in meter) and s, double matrix $(N \times 3)$ for the position coordinates of measurements (in meters).

Outputs :H (Electric Lead Field matrix)

Called by : Command line

A.1.5 mat_bemforward.dll - Matlab - C interface function

Calculates forward potentials using BEM with COG.

Inputs : r double vector (3×1) for dipole cooordinates, $sIndex$ integer vector $(N \times 1)$ Indexing the dipole cooordinates, $sigma$ double vector $(Layers \times 1)$ for conductivities, CoG double vector $(N1+N2+..+NJ) \times 3$ for the center of gravity coordinates of triangles, $Triangles$ integer vector $(Layers \times 1)$ for the number of triangles at each surface, B double matrix of the inverse of the solid angle matrix, $B3$ double matrix of the inverse of the solid angle submatrix.

Outputs : W double vector for lead field matrix((N1+N2+..+NJ))

Called by : newrapmusic.m, realmusic.m

A.1.6 mat_incogbem.dll - Matlab - C interface function

Calculates the inverses of deflated solid angle matrixes using LU decomposition.

Inputs :$VertTri$, ineteger matrix containing the number of vertices and triangles per each surface, $Vertices$ $N \times 3$ vector for position of N vertices, $Triangles$, $M \times 3$ index of vertices in order to define triangles, $sigma$ is the parameter that contains the conductivity values of the surfaces.

Outputs : Cog $N \times 3$ vector which contains the centre of gravity of the triangles, $B3$ is the inverse of the submatrix of the solid angle, B is the matrix which contains the inverse of the total solid angle matrix.

Called by :Command line

A.1.7 inv_main.exe - Executable code to execute calculation inversion of Solid angle matrix

Calculates the centre of gravity of triangles, deflated dolid angle matrix, deflated solid angle submatrix and inverses of these matrixes for the boundary element method for the forward solution of electric potentials based on a tessellated head model.

Inputs : Binary file which has a data structure as Number of $Triangles$, Number of $Vertices$ per each surface. The coordinates of the *vertices* and the coordinates of the *triangles*.

Outputs :Cog.dat B.dat B3.dat Binv.dat B3inv.dat files which contains CoG, deflated solid angle, deflated solid angle submatrix, inverse of the deflated solid angle and inverse of the deflated solid angle submatrix variables.

Called by : Executable file, Operating System Shell

A.1.8 mat_musicbem.dll - Matlab - C interface function

Performs MUSIC scanning algorithm for the inverse solution of dipole position parameters.

Inputs : $sIndex$, index of the electrodes based on CoG coordinates, CoG centre of gravity values of triangles, $Triangles$ number of triangles per surface, B inverse of the deflated solid angle matrix, $B3$ inverse of the deflated solid angle submatrix, R selected coordinates of the head model, v is the measured EEG time series data, $EPSILON$ is a threshold value, $inputFileName$ is the name of the file that contains previously calculated eigenvalues and eigenvectors.

Outputs : $V1$, double vector ($Totalpixels \times 1$) for the MUSIC SPECTRUM of

the pixels in the volume $V2$, double vector ($Totalpixels \times 1$) for the number of dipoles in each pixel in the volume

Called by : realmusic.m, newrapmusic.m

A.1.9 mat_musicShellW.dll - Matlab - C interface function

Performs the singular value decomposition of gain matrices for the inverse solution of dipole position parameters using analytical shell approach and storing the results in a file.

Inputs : $sIndex$: index of the electrodes based on CoG coordinates, CoG, (in meters) centre of gravity parameters, R (in meters) selected coordinates of the head model, $fname$: is the file name parameter.

Outputs : The $fname$ file which contains the singular value decomposition of gain matrix regarding to the R points.

Called by :Command line

A.1.10 mat_musicShell.dll - Matlab - C interface function

Performs MUSIC scanning algorithm for the inverse solution of dipole position parameters using analytical shell approach for the forward problem.

Inputs : $sIndex$: index of the electrodes based on CoG coordinates, CoG,(in meters) centre of gravity parameters, R, (in meters) selected coordinates of the head model, $fname$, is the file name parameter, v is the time series EEG data, $epsilon$ as threshold value.

Outputs :

Called by :Command Line

A.1.11 mat_musicbemW.dll - Matlab - C interface function

Performs singular value decomposition of the gain matrix for each point of R and record the results in a file.

Inputs : $sIndex$, index of the electrodes based on CoG coordinates, CoG (in meters) centre of gravity values of triangles, $Triangles$ number of triangles per surface, B inverse of the deflated solid angle matrix, $B3$ inverse of the deflated solid angle submatrix, R selected coordinates of the head model, v is the measured EEG time series data, $EPSILON$ is a threshold value, $inputFileName$ is the name of the file that is going to contain eigenvalues and eigenvectors of the gain matrix.

Outputs :$V1$ is the double vector $Totalpixels \times 1$ for the MUSIC SPECTRUM of the pixels in the volume, $V2$ is the double vector $Totalpixels \times 1$ for the number of dipoles in each pixel in the volume.

Called by :Command Line

A.1.12 mat_musicbemnew.dll - Matlab - C interface function

Performs MUSIC scanning algorithm for the inverse solution of dipole position parameters with computing all steps without reading from a file.

Inputs : $sIndex$, index of the electrodes based on CoG coordinates, CoG (in meters) centre of gravity values of triangles, $Triangles$ number of triangles per surface,

B inverse of the deflated solid angle matrix, $B3$ inverse of the deflated solid angle submatrix, R (in meters) selected coordinates of the head model, v is the measured EEG time series data, $EPSILON$ is a threshold value.

Outputs :$V1$ is the double vector $Totalpixels \times 1$ for the MUSIC SPECTRUM of the pixels in the volume, $V2$ is the double vector $Totalpixels \times 1$ for the number of dipoles in each pixel in the volume.

Called by :mat_musicbemnew.dll

A.1.13 funIncRes.m -Matlab code that carries out the generation of points for the brain

Creates a new volume set according to parameters.

Inputs : R is the position of the voxel in MNI coordinate system, $totalPoints$ is the number of points in one line, $voxelSize$ is the length of the original voxels, $brain$ is the MRI data.

Outputs : R is the increased resolution volume

Calls : pixel2mni.m, mni2pixel.m

Called by :newrapmusic.m

A.1.14 mni2pixel.m -Matlab code that converts MNI coordinates to pixel coordinates

Converts the input MNI coordinates to pixel.

Inputs : $y1$ is the input MNI coordinates

Outputs : $y1$ is the pixel coordinates.

Calls :None

Called by : funIncRes.m

A.1.15 pixel2mni.m -Matlab code that converts pixel coordinates to MNI coordinates

Converts the input pixel coordinates to MNI coordinates.

Inputs: $y1$ is the input pixel coordinates

Outputs : $y1$ is the MNI coordinates.

Calls :None

Called by : funIncRes.m

A.1.16 vertplot.m -Matlab code that plots the data

Plots the data channels vertically.

Inputs:x is the data that is going to be plotted, *scale* is the integer parameter which is the step scale of the channels, h is the parent axes property of the graphical user interface on which the axes object exists, *cmenu* is the menu object name, $ProfileVar$ is the specific profile variable.

Outputs :

Calls :None

Called by :den1.m

A.1.17 xyz2pixel.m -Matlab code that converts the coordinates

Converts the xyz coordinates to binary images.

Inputs:R, xyz coordinates, L number of points in each slice, N sampling rate, $[m, n, q]$ is the dimensions of the original image.

Outputs : X is the pixel coordinates.

Calls :None

Called by :dipolpot.m

A.1.18 mrplot.m -Matlab code plots the results of MUSIC algorithm

Plots the dipole position onto the MRI data.

Inputs:z, xyz coordinates, $avg152brain$ brain mr data, R volume of coordinates (MNI), b is the result of the algorithm image(index of R), $Order$ is the number of dipoles, res is the time index of the data, SR is the caption of the figure.

Outputs :figure

Calls :None

Called by :dipolpot.m, newrapmusic.m

A.1.19 Newrapmusic.m -Matlab code that implements MUSIC algorithm

Implements MUSIC algorithm and returns the results graphically.

Inputs:CoG (in mm)is the centre of gravity values of the triangles, $Triangles$ is the vector containing the number of triangles per layer, $Binv\_elec$ is the inverse of the deflated solid angle matrix including only the necessary rows, $B3inv$ is the inverse of the solid angle submatrix, R (in mm) is the solution space that would be searched, Y is the EEG data, L is the number of points in each slice, $avg152brain$ is the brain mr data, $Order$ is the estimated number of dipoles, $Epsilon$ is the float parameter that helps to determine the number of dipoles, $ConvertPos$ is the order of the electrode system according to the 10-20 electrode system, $fName$ is the name of the file which was computed for the solution of Inverse problem, $timePos$ is the index of the EEG time which would be used for input data.

Outputs :

Calls :mat_musicbem.dll, funIncRes.m, mat_musicbemnew.dll ,mat_bemforward.dll, mrplot.m

Called by :den1.m

APPENDIX B. CD-ROM

The programs mentioned in Appendix A are found in CD-ROM, which is enclosed inside back cover. Minimum system requirements : Matlab V6 (Release 12), C++ Compiler, a pentium based PC with at least 128 MB RAM.

REFERENCES

1. Jr, O. W. W., L. J. D, S. J. A, and H. M. F, *Functional Brain Imaging*, Mosby, St. Louis, 1995.

2. Hoey, G. V., J. D. Clerck, B. Vanrumste, R. V. de Walle, I. Lemahieu, M. D'Have, and P. Boon, "EEG dipole source localization using artificial neural networks," *Phys. Med. Biol.*, Vol. 45, pp. 997–1011, April 2000.

3. Sun, M., "An efficient alorithm for computing multishell spherical volume conductor models in EEG dipole source localization," *IEEE Trans. On Biomedical Eng.*, Vol. 44, pp. 1243–1252, December 1997.

4. S.Hamalainen, M., and J. Sarvas, "Realistic conductivity geometry model of the human head for interpretation of neuromagnetic data," *IEEE Trans. On Biomedical Eng.*, Vol. 36, pp. 165–171, February 1989.

5. Koles, Z. J., "Trends in EEG source localization," *Electroencephalograpy and clinical Neurophysiology*, no. 106, pp. 127–137, 1998.

6. J.P., A., K. S.A., and F. D.H., "Location of sources of evoked scalp potentials:corrections for skull and scalp thickness.," *IEEE Trans. Biomed Eng.*, Vol. 6, pp. 447–452, 1981.

7. M., R., T. R., and A. S., "Numerical solution of the potential due to dipole sources in volume conductors with arbitrary geometry and conductivity.," *IEEE Trans. Biomed Eng.*, Vol. 43, pp. 679–689, 1996.

8. Wilson, F., and R. H. Bailey, "The electrical field of an eccentric dipole in a homogeneous spherical conducting medium," *Circ*, Vol. 1, pp. 84–92, 1950.

9. Rush, S., and D. A. Driscoll, "Current distribution in the brain from surface electrodes," *Anesth. Analg.*, Vol. 47, pp. 717–723, 1968.

10. Stok, C. J., *The Inverse Problem in EEG and MEG with Application to Visual Evoked Responses.* PhD thesis, University of Twente, Netherlands, 1986.

11. Heinonen, T., H. Eskola, P. Dastidar, P. Laarne, and J. Malmivuo., "Segmentation of t1 mr scans for reconstruction of resistive head models," *Computer Methods and Programs in Biomedicine.*, Vol. 54, pp. 173–181, 1997.

12. Ademoglu, A., T. Demiralp, Y. Istefanopulos, S. Comu, and B. Baykan, "Epileptic source localization using wavelet prefiltering and MUSIC scanning," *IEEE-EMBC.* Mexica,17-21 September, pp. 2366-2369, 2003.

13. Schlitt, H. A., L. Heller, R. Aaron, E. Best, and D. M.Ranken, "Evaluation of boundary element methods for the EEG forward problem: Effect of linear interpolation," *IEEE Trans. On Biomedical Eng.*, Vol. 42, pp. 52–57, January 1995.

14. Sarvas, J., "Basic mathematical and electromagnetic concepts of the biomagnetic inverse problem," *Physics in Medicine and Biology*, Vol. 32, pp. 11–22, 1987.

15. Oosterom, A. V., and J. Strackee, "The solid angle of a plane triangle," *IEEE Trans. On Biomedical Eng.*, Vol. 30, pp. 125–126, February 1983.

16. Lynn, M. S., and W. P. Timlake, "The use of multiple deflations in the numerical solution of singular systems of equations , with applications to potential theory," *SIAM J. Numer. Anal.*, Vol. 5, no. 2, 1968.

17. Plonsey, R., "Reciprocity applied to volume conductors and the EEG," *IEEE Trans. On Biomedical Eng.*, Vol. 10, pp. 9–12, 1963.

18. Vanrumste, B., *EEG Dipole Source Analysis In a Realistic Head Model.* PhD thesis, Gent University, Gent, Belgium, 2001.

19. Marquardt, D. W., "An algorithm for least-squares estimation of non-linear parameters," *Jour Soc Indust. Appl. Math*, Vol. 11, pp. 431–441, 1963.

20. Press, W. H., B. P. Flannery, S. A. Teukolsky, and W. T. Vetterling, "Minimization or maximization of functions," in *Numerical Recipes, The art of scientific computing*, ch. 10, pp. 439–443, New York: NY Cambrige Univ Press, 2 nd ed., 1992.

21. Koles, Z. J., J. C. Lind, and A. C. Soong, "Spatio-temporal decomposition of the EEG : a general aproach to the isolation and localization of sources," *Electroencephalograpy and clinical Neurophysiology*, Vol. 95, pp. 219–230, 1995.

22. Koles, Z. J., and A. C. Soong, "EEG source localization: implementing the spatio temporal decomposition approach," *Electroencephalograpy and clinical Neurophysiology*, 1998.

23. Mosher, J. C., "Recursively applied MUSIC (RAP-MUSIC), MEG and EEG for human brain mapping , fundamentals through advanced issues.," *Proceedings 2nd International Conference on Functional Mapping of the Human Brain*, Boston,1996.

24. Mosher, J. C., P. S. Lewis, and R. M.Leahey, "Multiple dipole modeling and localization from spatio-temporal meg data," *IEEE Trans. On Biomedical Eng.*, Vol. 39, pp. 541–557, June 1992.

25. Meijs, J. W.H., Weier, W. Onno, Peters, J. Maria, van Oosterom, and Adriaan, "On the numerical accuracy of the boundary element method," *IEEE Trans. Biomed Eng.*, Vol. 36, pp. 1038–1049, 1989.